Mathematical Modeling and Characteristics Analysis of Ultra-Wideband *In vivo* Radio Channel

by

Muhammad Ilyas

Electrical and Computer Engineering

Submitted to the Graduate School of Science and Engineering

in partial fulfillment of the requirements for the degree of

Doctor of Philosophy

ALTINBAŞ UNIVERSITY

2018

This is to certify that we have read this thesis and that in our opinion it is fully adequate, in scope and quality, as a thesis for the degree of Doctor of Philosophy.

Assoc. Prof. Oguz BAYAT

Supervisor

Examining Committee Members (first name belongs to the chairperson of the jury and the second name belongs to supervisor)

Prof. Osman Nuri UCAN	School of Engineering and Natural Sciences, Altinbas University	_____
Assoc. Prof. Oguz BAYAT	School of Engineering and Natural Sciences, Altinbas University	_____
Asst. Prof. Cagatay AYDIN	School of Engineering and Natural Sciences, Altinbas University	_____
Prof. Hasan Huseyin BALIK	School of Engineering, National Defense University	_____
Asst. Prof. Adil Deniz DURU	Faculty of Sport Sciences, Marmara University	_____

I certify that this thesis satisfies all the requirements as a thesis for the degree of Doctor of Philosophy.

Asst. Prof. Cagatay AYDIN

Head of Department

Approval Date of Graduate School of Science and Engineering: ____/____/____

Assoc. Prof. Oguz BAYAT

Director

I hereby declare that all information in this document has been obtained and presented in accordance with academic rules and ethical conduct. I also declare that, as required by these rules and conduct, I have fully cited and referenced all material and results that are not original to this work.

Muhammad Ilyas

DEDICATION

This study is wholeheartedly dedicated to my beloved wife and parents, who have been my source of inspiration and strength.

To my brothers, sister, mentor, professors and classmates who shared their opinions and advice to finish this study.

Above all, To the almighty God!

ACKNOWLEDGEMENTS

I wish to express my sincere gratitude to all my Professors especially, Assoc. Prof. Dr. Oguz Bayat for his continues guidance, Asst. Prof. Dr. Qammer H. Abbasi for his time, guidance and un conditional support and Prof. Dr. Osman Nuri Ucan for showing me the path by using his experience.

I am also indebted to the Graduate School of Science and Engineering staff and students, Altinbas University, for their support and cooperation.

Finally, I would like to thanks all my co-authors in all my publications for their support and guidance which help me complete my research.

ABSTRACT

Mathematical Modeling and Characteristics Analysis of Ultra-Wideband *In vivo* Radio Channel

Ilyas, Muhammad,

PhD, Electrical and Computer Engineering, Altınbaş University,

Supervisor: Assoc. Prof. Dr. Oguz Bayat

Date: August 2018

Pages: 82

In this research, we present the experimental analysis of *in vivo* wireless channel response on Ultra-Wideband (UWB) with the frequencies between 3.1 – 10.6 GHz. The analysis proves the location dependent based characteristics of *in vivo* channel. The results clearly show the highly multipath scenario. It can also be observed that the multipath effect of the channel is much higher in the denser areas, i.e. an antenna placed within the intestine area or inside the stomach. which is used as a reference model for *in vivo* channel response without performing intensive experiments or simulations. The statistics of error prediction between experimental and proposed model is RMSE = 5.29, which show the high accuracy of the proposed model. In addition, the proposed model was applied on the blind data and the statistics of error prediction is RMSE = 7.76, which also shows a reasonable accuracy of the model. This model will save the time and cost on simulations, experiments and will help in designing an accurate link budget calculation for future enhanced system.

This study also presents bit error rate (BER) performance analysis and improvement using equalizers for an *in vivo* radio channel. By conducting simulations using a bandwidth (BW) of 50 MHz, we observed that the *in vivo* radio channel is affected by small-scale fading. This fading results in inter-symbol interference (ISI) affecting upcoming symbol transmission, causing delayed versions of the symbols to arrive at the receiver side and causes increase in BER. A 29 taps channel was observed from the experimentally measured data using a human cadaver and BER was calculated for the measured *in* vivo channel response along with the ideal additive white Gaussian noise (AWGN) and Rayleigh channel models. Linear and non-linear adaptive equalizers i.e., decision feedback equalizer (DFE) and least mean square (LMS) were used to improve the BER performance of the *in* vivo radio channel. It is noticed that both the equalizers improve the BER, but DFE has better BER compared to LMS and shows a 2 dB and 4 dB performance gain of DFE over the LMS at Eb/No = 12 dB and at Eb/No = 14 dB, respectively.

Keywords: Bit Error Rate, Channel Characterization, Channel Response, Equalization, Implantable/Wearable Devices, *In-vivo* Channel, *In-vivo* Communication, Mathematical Modeling, Wireless Body Area Networks, Ultra-Wideband.

TABLE OF CONTENTS

Pages

LIST OF TABLES

Pages

LIST OF FIGURES

Pages

LIST OF ABBREVIATIONS

LOS:	Line of Sight
RF:	Radio Frequency
MSE:	Mean Squared Error
MMSE:	Minimum Mean Squared Error
MATLAB:	Matrix Laboratory
PDF:	Probability Density Function
NLOS:	Non Line of Sight
UWB:	Ultra-Wideband
WBAN:	Wireless Body Area Network
UMTS:	Universal Mobile Telecommunication System
LTE:	Long Term Evolution
Wi-Fi:	Wireless Fidelity
5G:	Fifth Generation
VNA:	Vector Network Analyzer
FFT:	Fast Fourier Transform
IFFT:	Inverse Fast Fourier Transform

OFDM:	Orthogonal Frequency Division Multiplexing
WSN:	Wireless Sensor Network
PAN:	Personal Area Network
TCP:	Transmission Control Protocol
IP:	Internet Protocol
CMOS:	Complementary Metal Oxide Semiconductor
BW:	Band Width
MHz:	Mega Hertz
GHz:	Giga Hertz
BER:	Bit Error Rate
MM:	Millimeter
THz:	Tera Hertz
CPW:	Coplanar Wave Guide
PDP:	Power Delay Profile
RMS:	Root Mean Square
IDFT:	Inverse Discrete Fourier Transform
ISI:	Inter Symbol Interference

RMSE: Root Mean Square Error

LMS: Least Mean Square

DFE: Decision Feedback Equalizer

IMD: Implantable Medical Device

RSS: Received Signal Strength

RSSI: Received Signal Strength Indication

SAR: Specific Absorption Rate

Mbps: Megabits Per Second

RLS: Recursive least square

MLSE: Maximum Likelihood Sequence Estimator

AWGN: Additive White Gaussian Noise

Bc: Coherence Bandwidth

Fc: Central Frequency

BPSK: Binary Phase Shift Keying

RRC: Root Raised Cosine

NB: Narrow Band

WB: Wide Band

PSD: Power Spectral Density

DTFT: Discrete Time Fourier Transform

QAM: Quadrature Amplitude Modulation

TD: Time Domain

FD: Frequency Domain

PSK: Phase Shift Keying

1 INTRODUCTION

Wireless communication technologies are developed over the subsequent years. There are different types of wireless technologies present today ranging from smart phones to Laptops, Bluetooth, Wi-Fi access points etc. In wireless communication the transmission toke place without using any physical medium but air using electromagnetic waves like RF, IR, satellite etc. Among all those wireless communication technologies there is a new emerging technology under research called *in vivo* communication.

1.1 IN VIVO COMMUNICATION

In vivo communication [1] is one of the most emerging technologies under research. It helps us understand the communication between implantable devices [2] placed inside the human body with external conventional communication devices using Universal Mobile Telecommunication System (UMTS), Long Term Evolution (LTE), Wireless Fidelity (Wi-Fi) or possibly Fifth Generation (5G) technologies in the near future. There are several devices under research to be implanted in a human body to wirelessly send data to the server or doctor in case of a patient with the implant. The hurdles in developing those devices are their size, which is expected to be possible on a micro or nanoscale [3], battery life, circuit design and antenna for communication. Besides all those challenges the most critical part is to extensively study and understand the channel for *in vivo* communication.

Wireless channel [4] is always hard to predict and analyze; it can quickly change according to the environment and position of the antennas especially in non-line of sight scenarios. We can consider a channel as a black box where we only know the input and what we received at the output. Although there are different channel models presented by the researchers for different types of wireless scenarios, for conventional communication [5] and non-conventional communication, i.e. *in-vivo* communication channel model [6].

The mobile wireless communication channel varies over time and frequency. This variation can be mainly divided into two types, large-scale fading [7] and small-scale fading [8]. Large-scale fading is the function of distance and shadowing by large objects such as buildings while on the other hand, small-scale fading occurs due to the constructive and destructive interference of a

multipath signal. In order to design an efficient system, it is essential to measure the channel extensively. The knowledge of the channel response allows us to build propagation models [9] and get the maximum out of the system.

1.2 WIRELESS BODY AREA NETWORKS

Wireless body area networks (WBAN's) Figure 1.1, have been under research for a few years now [10-14]. Constant assessment of physiological parameters, particularly in chronic diseases including cardiac failure, asthma, bipolar mood disorder and diabetes, can provide insight into disease progression over time and assist healthcare providers in making the best therapeutic decisions.

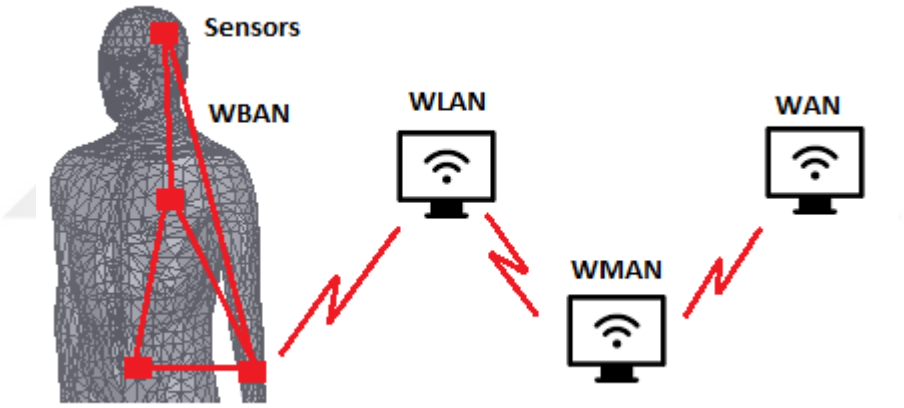

Figure 1.1. Wireless body area network

Personal heath monitoring systems are developed to continuously monitor human health by placing sensors on them and getting real time reading from the patients [15]. There are number of personal health monitoring devices available in the market and some of them are still under research some of the devices can be seen in Figure 1.2. Previous studies have been performed on heterogeneous sensor networks, which combine wireless sensor networks (WSN's) and personal area networks (PAN's) using a transmission control protocol/internet protocol (TCP/IP) [16]. Due to the low power requirements of WBAN's low power control protocols are needed for the communication [19]. Physical layer for WBAN has also been studied using complementary

metal oxide semiconductor (CMOS) in which the human body was used as a communication channel to transfer data [17].

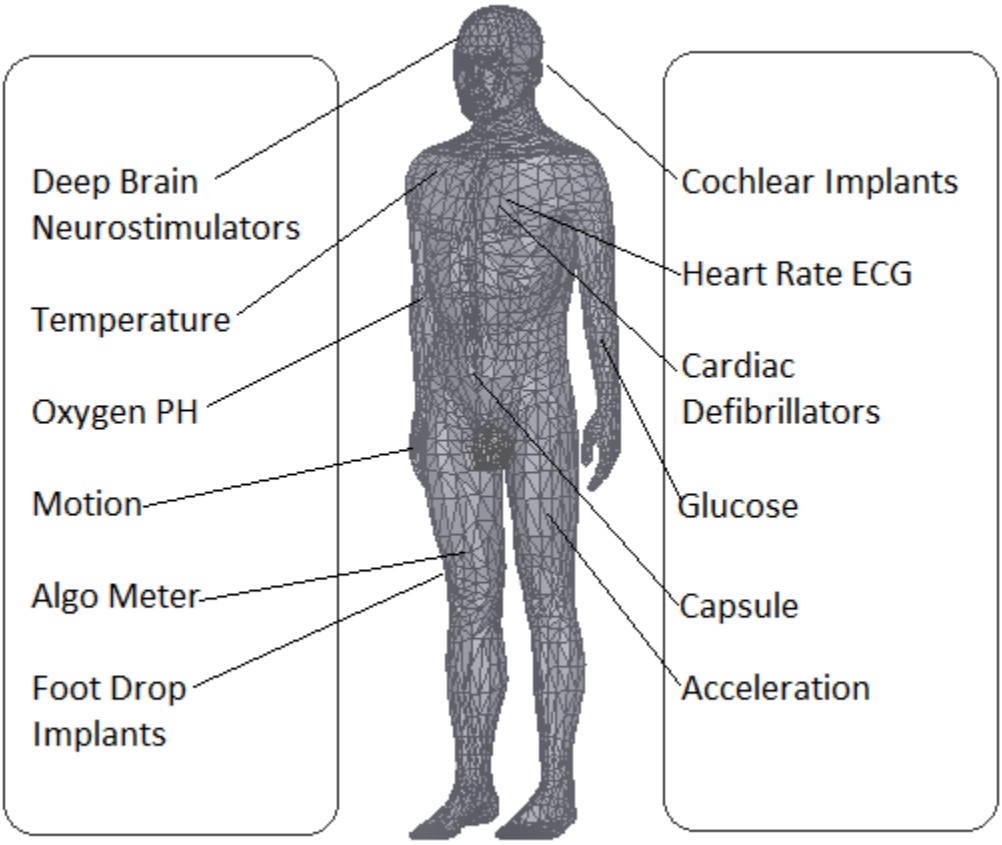

Figure 1.2: Patient with possible Implantable devices

In some cases, due to strategic placement, the sensors on the body are required to send large amount of data quickly. This requires Ultra-wide band (UWB) communication [18] but due to UWB, inter symbol interference (ISI) can be observed especially with Band width (BW) of more than 500 megahertz (MHz). Multipath fading [20] is a major problem in indoor environments and short distance communication especially in the presence of other objects like desk, chairs, walls and electronic equipment. This results in reflection, refraction, dispersion and diffraction of the signal and results in multipath small and long scale fading. Signaling fading can also occur to varying degrees depending on antenna propagation [21], the way a signal propagates. For

instance, the multipath fading effect is less significant with directional antennas, when compared to an Omni directional antenna. Researchers are trying their best to come up with different types of channel characteristics and path loss models [23] to improve the communication and make it more secure and risk free.

Many studies utilize the use of live animals to better understand the use of implantable devices and *in vivo* communication for collecting physiologically relevant recordings and data. Anzai *et al.* [22] conducted experiments on animals using UWB impulse radio, which resulted in a path of 80dB and a bit error rate (BER) of 10^{-2} within the distance of 120mm, with a high data rate of 1Mb/s. In [24], Propagation model was proposed for UWB body centric wireless communication. BER performance were also measured using multiband orthogonal frequency division multiplexing (OFDM). *In vivo* channel model in body centric wireless communication is also presented and explained in [25]. Path loss models [26] are explained and presented using different frequencies by simulations and real experiments using animals and human bodies by placing the sensors on top of the body. Wireless capsules are used to get the human data from inside the body by studying variations of path losses [27].

Different types of implantable and wearable devices [28] - [30] have been the focus of many research articles in recent years Figure 1.3. Few of the latest research are expending the implantable technology to the Nano scale for which the frequencies they are selecting and considering the best are in terahertz range. In [31], terahertz channel characteristics under human skin are presented using measurement data and modeled data is shown. Analytical characteristics of terahertz in Nano communications are also studied by R. Zhang et al, in [32]. Although there are some studies showing the characteristics and analysis of *in vivo* channels, most of them are limited to simulations and models based on assumptions or by using experiments only. To the best of author's knowledge, there are no explicit investigation performed to present a generic mathematical model and applying it to the experimental measurements with high accuracy. In this paper we presented a novel mathematical model for *in vivo* radio channel at UWB with a highest accuracy of RMSE = 5.297, while applied on the channel response extracted from experimental data. Additionally, blind testing is performed on the proposed model for validating the analytical results with the simulated data. This novel mathematical model will save the cost and time on simulation and measurements for UWB *in vivo* radio channel.

Figure 1.3: Wearable devices

1.3 IMPLANTABLE DEVICES

Implantable devices are under research for a while now, and researchers make it possible to commercialize most of the devices including cardiac pacemakers, drug delivery and defibrillators [10] - [33]. However, the size of the implantable devices is always an issue, and scientists are continuously working to make it smaller, and design micro antennas [34] for the successful communication with the outside wireless devices plus it will help reduce the size of the implantable device. As any electronic device, these devices need stable power required to work correctly and charging them or changing their batteries is an issue. Due to this implanted nature, power efficient [35] devices need to be designed for the successful communication. Experiments have been performed to check if these devices can be charged wirelessly [36]. In [37] an option is presented which uses human motion to recharge the device. To transfer data to the central system or from one node to another node, those devices commonly use the wireless channel, and as this important data is sent wirelessly, it is vulnerable and at risk of attacks by an outside intruder. The communication between implantable devices must be encrypted and secured [38] enough to safely transfer the data. Semantic wireless attacks are performed and tested in [39], and it is shown that the low power and cheaper medical devices are at high risk. Considering the

requirements of low power and high data rates, UWB communication can help provide reasonable bandwidths plus low power consumption. Experimental analysis or UWB path loss model is presented in [40]. Different channel models for implantable medical devices (IMD's) are discussed in [41], and the commercial deployment of these devices are discussed in [42]. According to the berg insight estimation it is expected that by 2021 medical monitoring devices will reach the Figure of 50 million as shown in the Figure 1.4.

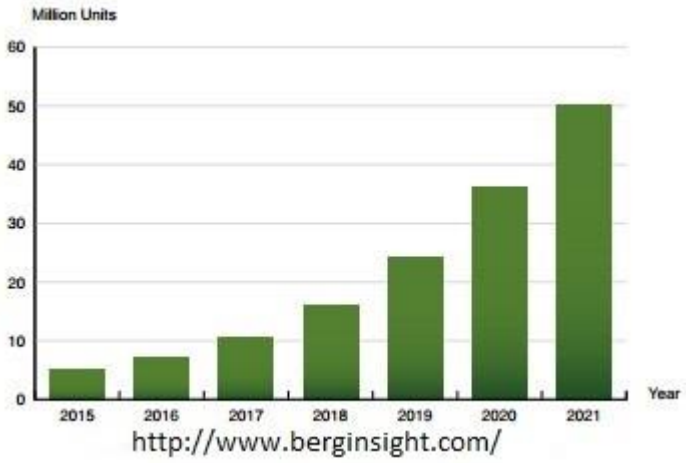

Figure 1.4: Connected home medical monitoring devices (2015-2021)

Multiple signal strength and impulse response tests were performed using a perfect human body model [43]. It is observed that the variations are more profound at high frequencies up to received signal strength (RSS) 20 dB. Blood vessels are used as a transport channel for i*n vivo* communication in [44], controlled information transfer through an *in vivo* nervous system is demonstrated using the neurons of an earthworm in [45]. In communication systems we always face errors on the receiver side, caused by multiple factors including effect of noise, outside environment, climate, multipath especially in indoor structures, reflection, diffraction, fading and interference due to the nearby wireless devices. These factors affect the signal and results in the degradation of bit error rate (BER). In [46] authors demonstrated the maximum allowed transmitted power from an *in vivo* device to achieve the desired BER while maintaining the specific absorption rate (SAR). The targeted data rates of 100 Mbps is achieved with maximum SAR which is the amount of radio frequency (RF) absorbed by the body [47]. To obtain a high data rate communication, UWB is still a good option due to its properties of low power and high bandwidth.

UWB channel is used in different areas of medical science for positioning and communication in the operating room [48] both in live (during operation) and non-live scenarios. It is observed that even within a highly multipath environment UWB provides reasonable results. UWB channel characteristics and system model is discussed in [49]. In communication system there is always a tradeoff to achieve high bandwidth with low power. The use of UWB introduces inter-symbol interference (ISI), which affects the performance of the system and thus results in high BER's. To avoid or improve the BER performance of UWB *in vivo* communication, using equalizers [50] is the best option. There are different types of equalizers present in the literature, they can be divided into two main types, adaptive linear and non-linear equalizers. The most effective linear equalizers are recursive least square (RLS) and least mean square (LMS) equalizers [51]. RLS and LMS can be used in combination by using their properties effectively [52]. On the other hand, the most common non-linear equalizers are decision feedback equalizer (DFE) and maximum likelihood sequence estimator (MLSE) equalizers. There are different types of DFE [53] equalizers available in the literature with their specific functions according to the requirement [54-56], such as to improve the BER and reduce ISI to get the desired signal at the receiver end. Channel coding is also used to improve the BER performance of the system but channels with high ISI first need to be equalized [57-59] to cancel or reduce ISI and then recovered using channel coding. This paper presents the BER analysis of experimental *in vivo* radio channel with and without equalization. for the first time in the literature as per author's knowledge. The channel response is compared with AWGN and Rayleigh channel. Furthermore, different types of equalizers (both linear and non-linear) are used to improve the BER performance. Overall, the equalizers improved the performance significantly. According to the results it is clear that non-linear equalizer outperformed the linear equalizer. DFE shows a 2 dB performance gain over the LMS at Eb/No = 12 dB and 4 dB at Eb/No = 14 dB.

The rest of the Thesis is organized as follow.

Chapter 2 discussed the experimental setup and simulations. experimental analysis of Ultra-Wideband (UWB) *in vivo* channel response. Simulations are presented for three different regions of the human body including heart, stomach and intestine in six different places.

Chapter 3 focuses on the proposed mathematical model along with the simulated measurement data results, followed by the blind testing for our proposed model using new data which was not previously used by our model.

Chapter 4 presents the bit error rate performance of experimental *in vivo* channel without using equalization and comparing it with ideal additive white Gaussian noise (AWGN) channel and ideal Rayleigh channel. Following up by the equalization techniques and use of equalizer along with the mathematical equations used for all the equalizers. The simulations of a BER performance for *in vivo* communication and spectrum of the un-equalized and equalized signals are also discussed and analyzed.

Finally, Chapter 5 concludes the thesis along with the summary of the results and contributions.

2 EXPERIMENTAL SETUP AND SIMULATIONS

This study is based on number of intensive experiments performed using a human cadaver. All the experiments were performed under the supervision of doctor who setup the cadaver for our use and helped us place *in* vivo antenna inside the cadaver as instructed throughout the experiments. Only the torso part of the cadaver is used for the experiments. The cadaver and tools used for the experiments can be seen in Figure 2.1. The tools consist of two antennas one *in vivo* used place inside the torso and one *ex vivo* used to be placed outside the human torso with different angles and distances. Cables used to connect the antennas with VNA (Vector Network Analyzer). Although the medium used between the two antennas is wireless so the communication between the *in vivo* and *ex vivo* antenna was wireless communication and both were sending data packets wirelessly. The antenna was also protected in order to avoid short circuit.

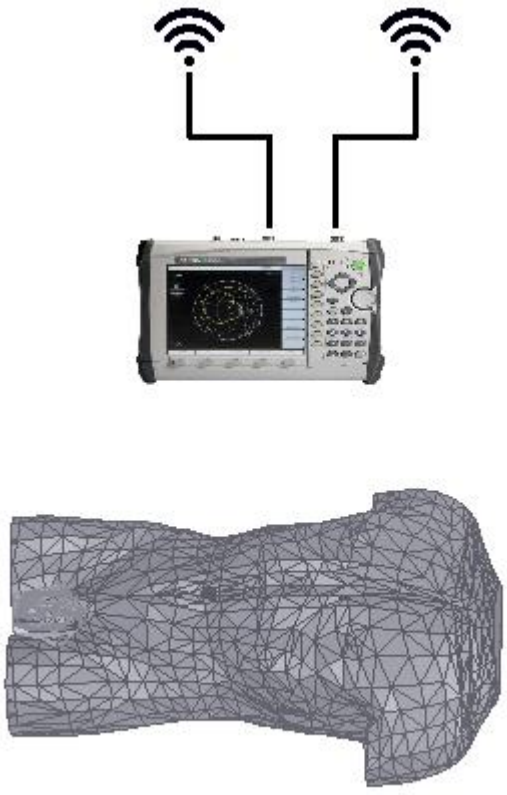

Figure 2.1: Cadaver and tools used in experiments

2.1 EXPERIMENTS

The experiments were performed using a human cadaver as presented in [60]. Only the torso part of the cadaver was taken into consideration and simulated in ANSYS-HFSS [61]. Two antennas were used in this experiment the first one is an *ex vivo* dipole antenna and the second one is a coplanar waveguide (CPW)-fed *in vivo* antenna. Compatible polyethylene protective layer [62] was used to wrap the antennas and part of the cable to avoid any physical connection with cadaver, organs, or tissues. All the experiments were performed under the assistance of certified medical doctor in a hospital after ethical approvals. In order to generate affective data, fresh organs such as heart, stomach and intestine from a sheep were used to place inside the human cadaver. The complete list of equipment's can be seen in Table 2.1.

Table 2.1: Equipment's used in experiments

Equipment/Subject	Values/Quantities
Measurement device	VNA
Cable	Coaxial
No of Antennas	2
Antenna Type 1	*Ex vivo*
Antenna Type 2	*In vivo*
Length of the cable	2 meters
Subject	Human Cadaver
Organs used	Heart, stomach and Intestine
Frequency	915MHz

Initially the equipment's were checked to make sure the system was working properly in order to avoid false reading the cable losses are calculated properly [60]. Two types of antennas were

used in the experiments an *in vivo* and an *ex vivo* antenna. *In vivo* antennas was used to place inside the human cadaver in different places including on top of heart, below heart, on top of stomach, inside stomach and below stomach and finally on top of intestine, inside intestine and below intestine. The *ex vivo* antennas were placed on the center of the body, near the head at the right lateral, left lateral. Extensive experiments were performed to collect the data, each experiment was performed multiple times and the average was taken to be used in simulations and mathematical modeling. A two-meter-long coaxial cable was used to connect the antennas with a vector network analyzer (VNA). The experimental setup can be seen in Figure 2.2.

In vivo antennas were placed in six different parts inside the human torso, including on top and beneath the heart, stomach, and intestines, whereas *ex vivo* antennas were placed outside the human torso, including near the head, beside the torso and near the foot to get different readings [60]. It was found that electromagnetic wave propagation was highly dependent on the location of the *in vivo* antenna, particularly if the antenna was placed deep inside the torso or within a dense region, like near the intestines. Furthermore, significant multipath and small-scale fading occurred during testing [60]. Antenna depth and path loss model for the experimental data compared to the simulated environment is presented in [23].

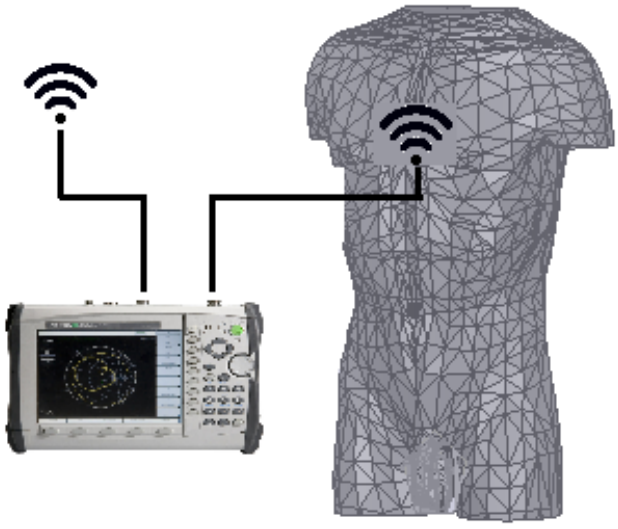

Figure 2.2. Experimental setup for UWB In-vivo measurements.

These experiments allow us to further our understanding of *in vivo* communication and channel characteristics, which could potentially help doctors and engineers better understand how waves

are propagating and the effect of fading while communicating wirelessly under real scenarios. The primary aim of this study is to provide a new tool for healthcare providers that allows constant monitoring of patients. The doctors will be able to follow his patient using wireless technology with the help of a device implanted in the human body, which actively collects and reports physiologically relevant data regarding the patient. The measurements will be automatically sent to the doctors through Wi-Fi, Bluetooth or GSM as shown in Figure 2.3. This information will allow patients and doctors to follow disease progression more accurately and thereby provide an opportunity for more effective and efficient care.

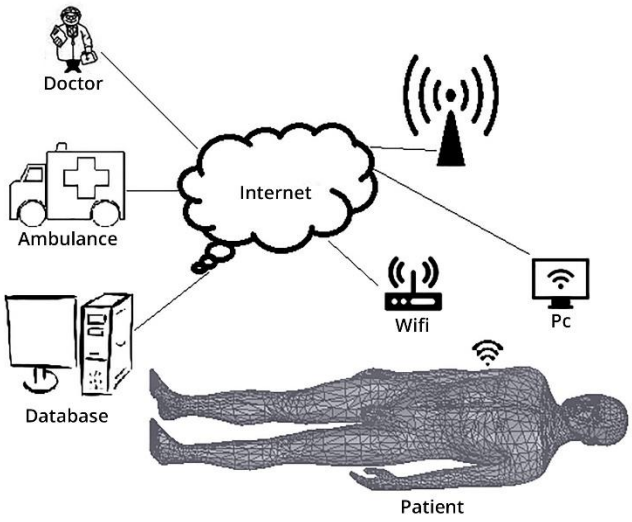

Figure 2.3: Envisaged patient system model with *in vivo* implant communicating through different conventional communication devices.

To get a real channel response, extensive experiments were performed using a human cadaver. Three locations were selected for the experiments. The heart area, stomach area and intestine. These locations were subdivided according to the requirements of the test by placing the antennas below, on top and inside the organs. To make it near to the real scenario, fresh animal organs were selected to be placed in the human cadaver. Two different types of antennas were used for those experiments, an *ex vivo* antenna and an *in vivo* antenna, both the antennas fully protected and covered to avoid any contact with organs. The *in vivo* antenna were placed inside the cadaver in different locations to get the readings while the *ex vivo* antenna position was fixed

for all those experiments. The depths, angles and losses for those experiments are presented in [60]. Demir *et al.* [23] presented a statistical path loss model and *in vivo* channel characteristics for a male torso, power delay profile of each anatomical direction is also simulated to understand the power losses.

2.2 SIMULATIONS

The channel response for the experiments were saved using a Vector Network Analyzer (VNA). Both the antennas were connected with the VNA. Simulations were carried out in Matrix Laboratory (MATLAB). Simulation parameters are shown in Table 2.2. The *in vivo* antenna was placed on top, below and inside the stomach. While for heart and intestine the antennas were only placed on top and below the heart and intestine. The data collected was normalized using eq. (1.1).

$$N_i = \frac{x_i - min(x)}{max(x) - min(x)} \tag{1.1}$$

Where $x = (x_1, \dots, x_n)$ and N_i is our i^{th} normalized data.

$min(x)$ is the minimum value of variable *x.*

$max(x)$ is the maximum value of variable *x.*

Table 2.2: Simulation parameters

Parameters	Values/units
Frequency to Time domain	IFFT
Bandwidth	50MHz
Central Frequency	6.75GHz
S-parameters	S_{21}
Time	μsec
Channel Response	Normalized (0-1)

The original data saved through VNA was in the frequency domain eq. (2.2) which has been converted to time domain eq. (2.3) using Inverse Fast Fourier Transform (IFFT). As we know that multiplication in frequency domain is equivalent to convolution in time domain. The data was collected at UWB frequencies (3.1 – 10.6 GHz), but for simulation, only 50 MHz bandwidth was selected, the central frequency for this UWB is 6.75GHz. Data was normalized between (0-1). The normalized channel response for stomach is shown in Figure 2.4. Figure 2.4 is showing readings in three different locations including below, on top of and inside the stomach. Figure 2.5 presents channel response for heart presenting readings in two different positions including below and on top of the heart. While Figure 2.6 confers the channel response for intestine conferring readings on top of and below intestine.

$$y(f) = H(f)x(f) \tag{2.2}$$

$$y(n) = H(n) \otimes x(n) \tag{2.3}$$

Here $H(f/n)$ is channel response, *x y H* are all functions of signal frequency *f/n.*

Simulations prove that even a slight change in the position of the *in vivo* antenna inside the human cadaver can affect the communication. It can also be observed that *in vivo* communication is highly location dependent and it is a highly multipath channel. As from the graphs, it is shown that channel response is highly unpredictable and can be easily changed with the movement of the antenna. As different places were selected inside the cadaver for the placement of the *in* vivo antenna, i.e. on top below and inside (in case of stomach only) to understand the *in vivo* channel.

The plots show that the multipath effects in the denser area are higher as compared to the comparatively non-denser areas. If we can observe the stomach plots the multipath effect and channel taps are much higher while the antenna is placed below or inside the stomach, as compared to the readings while the antenna was placed on top of the stomach. Those situations can also be observed in heart and intestine plots. The multipath effect is much higher while the antenna is placed below the heart. For intestine overall, the multipath effect is much higher as

compared to the heart plot. As intestine itself creates a perfectly dense situation for the signal to travel, and high power is required to place an antenna inside or below the intestine as compared to the other parts. In all experiment, the skin of the human cadaver was kept closed while taking the readings which add another layer of protection for the signal.

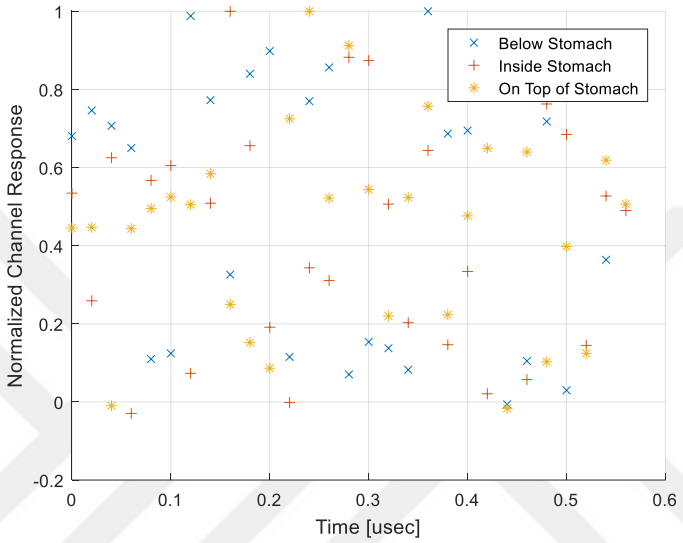

Figure 2.4: Normalized channel response for the stomach.

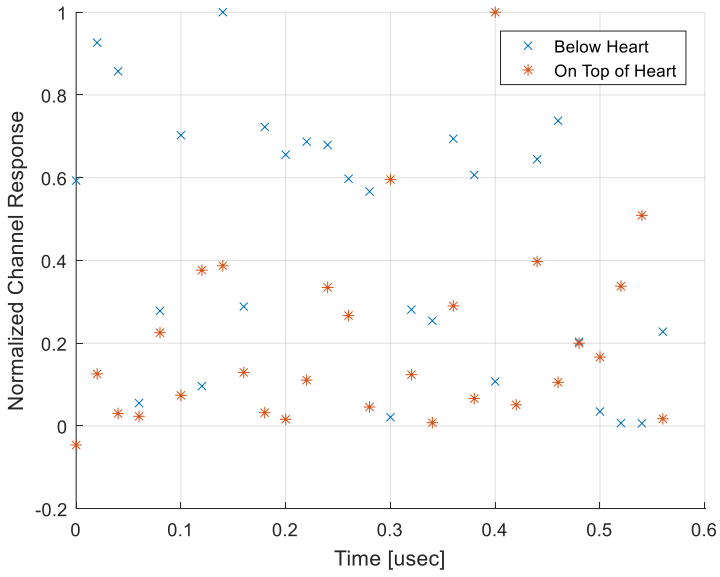

Figure 2.5: Normalized channel response for heart.

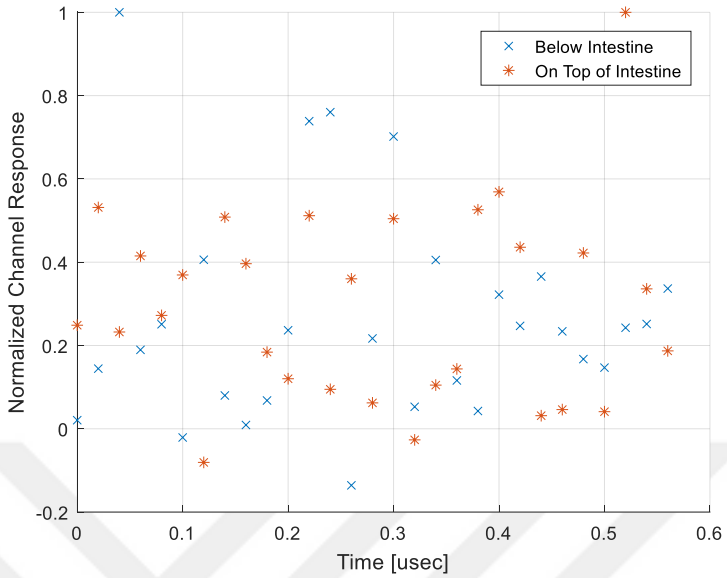

Figure 2.6: Normalized channel response for intestine.

The simulations will help the researchers understand the real channel response and its effects on the communication. It is concluded that *in vivo* is a multipath channel and can be highly changeable with the change in position of the antenna even if it is at a small distance. The reported analysis highlights the challenges for modelling those types of channels and open a way for further studies in such environment.

3 MATHEMATICAL MODELING

There are number of extensive and time consuming experiments were performed to extract the data by using the real scenario closed to the human body. It is realized that for additional results repeating those experiments is a hard job as there is extensive legal documentations is required to get permission to access a cadaver under the supervision of certified medical doctor. It is decided to design a mathematical model by using the experiments which will help future researchers to use the model by considering the errors between the real data and the proposed model to avoid time consuming experiments. The following terms need to be clarified used in the mathematical modeling.

3.1 SMALL SCALE FADING

Small scale fading is used to describe the fading in which the rapid fluctuation of the amplitude and phase is noticed for a short period of time. It is also due to the result of multipath which is caused by interference between two or more signals of the transmitter received with different time intervals at the receiver. Small scale fading is normally observed in the dense area or mostly in the indoor structures as the transmitted signal is arriving to the receiver at different time intervals due to reflection from walls and stuff inside the structure.

3.2 DELAY SPREAD

Delay spread or the RMS delay spread is the root mean square value of the delay of the reflections weighted proportional to the energy of the received signal or pulses.

3.3 POWER DELAY PROFILE

The power delay profile (PDP) gives the distribution of signal power received over a multipath channel as a function of propagation delays. It is obtained in [4]. Mean excess delay ($\bar{\tau}$) and RMS delay spread (σ_τ) are the two most commonly used parameters for the time dispersive properties of wide band multipath channels [4]. Mean excess delay is defined as eq. (3.1).

$$\bar{\tau}=\frac{\sum_k p(\tau_k)\tau_k}{\sum_k p(\tau_k)} \tag{3.1}$$

The RMS delay spread is defined as eq. (3.2)

$$\sigma_\tau = \sqrt{\overline{\tau^2} - (\bar{\tau})^2} \tag{3.2}$$

Where

$$\overline{\tau^2} = \frac{\sum_k p(\tau_k)\tau_k{}^2}{\sum_k p(\tau_k)} \tag{3.3}$$

3.4 FOURIER TRANSFORM

Fourier transform is used to break the waveform in a function or signal into an alternative representation characterized by sines and cosines. It shows us that waveform can be re written as a sum of sinusoidal waves.

3.5 INVERSE DISCRETE FOURIER TRANSFORM

Inverse Discrete Fourier Transform (IDFT) is used to map the signal in frequency domain to time domain. It basically changes the representation of the signal from frequency to time domain. The time domain signal consists of the real values, where each value will represent the associated time. The inverse Fourier transform will take the original frequency series of the complex values and map it back to the time series, assuming that the original time series consist of real values and the result of IDFT will be complex numbers.

3.6 FOURIER SERIES

Fourier series can be describe as the expansion of infinite sum of the periodic function $f(x)$ in terms of sines and cosines. For the functions which are not periodic the Fourier series can be replaced by Fourier transform.

The Fourier series of a periodic function $f(x)$ of period T can be represented as eq. (3.4)

$$f(x) = \frac{a_o}{2} + \sum_{k=1}^{\infty} a_k \cos\frac{2\pi kx}{T} + \sum_{k=1}^{\infty} b_k \sin\frac{2\pi kx}{T} \tag{3.4}$$

For the Fourier coefficients a_k and b_k can be define as eq. (3.5) and eq. (3.6)

$$a_k = \frac{2}{T}\int_0^T f(x)\cos\frac{2\pi kx}{T}dx \tag{3.5}$$

$$b_k = \frac{2}{T}\int_0^T f(x)\sin\frac{2\pi kx}{T}dx \tag{3.6}$$

3.7 CONFIDENCE INTERVAL

Confidence interval (CI) is used to get an estimate of the huge data by taking a portion of that data to have an estimate range of values which is likely to include an un known population parameter.

3.7.1 Confidence levels

Confidence intervals are constructed at a confidence level such as 95%, selected by the user. It explains that if the statistics of the set of numbers has taken using 95% confidence internal the results can be considering is true for 95 cases out of 100.

3.8 SUM OF SQUARES ERROR

Sum of squares error is the sum of the squared differences between each observations and its group mean. It is used to get the measure of variation within the same cluster of data. In case of identical cases within the cluster the SSE will be equal to 0.

The equation used to calculate SSE is eq. (3.7)

$$SSE = \sum_{i=1}^{n}(x_i - \bar{x})^2 \tag{3.7}$$

3.9 ROOT SQUARE

Root square defines how good is the fit in explaining the variation of data. It is the square of correlation between the response values and the predicted response values.

R-squared is define as eq. (3.8)

$$R - squared = 1 - \frac{\left[Sum_{(i=1\ to\ n)}\{w_i(y_i - f_i)^2\}\right]}{\left[Sum_{(i=1\ to\ n)}\{w_i(y_i - y_{av})^2\}\right]} \tag{3.8}$$

Here

f_i is the predicted value from the fit

y_{av} is the mean of the observed data y_i

w_i represents the weights

3.10 ROOT MEAN SQUARE ERROR

Root Mean Square Error (RMSE) is the standard deviation of the prediction errors also called as residuals which are the measure of how far the data points are from the regression line. It shows us how concentrated the data is around the best fit. The equation presenting the RMSE is eq. (3.9)

$$RMSE = \sqrt{\overline{(f - 0)^2}} \tag{3.9}$$

Where

f = expected values

0 = known results

The bar represents the mean.

3.11 WEIGHTS

Weight variables provide the values for all the observations with in the data set. Most of the time the valid weight is positive, while a zero weight means that the observation is excluded from the analysis. Observations that have large weights has more impact I the analysis as compare to the observation that has less weights. Un weighted analysis are the same as weighted analysis where all the weights are 1.

3.12 DERIVATION OF THE MODEL

To correctly understand the multipath propagation and waveform design the amount of delay spread must be evaluated since this information is essential in designing a better *in vivo* communication system. It is shown in [23] that the tissues of the human body cannot absorb the EM waves completely, which contribute to small-scale fading over short distances.

The channel response was extracted from the measurement data. The channel impulse response, *h(t),* is derived by taking the Inverse Discrete Fourier Transform (IDFT) of the channel frequency response, S_{21}in MATLAB. The parameter of the simulation is shown in Table 2.2 chapter 2. Figure 3.1 shows the channel response for BW=50 MHz, theoretically it can be stated that ISI is not a big issue for low BW's, however, it can cause problems for higher BW's, which require a complex equalizer to deal with the ISI.

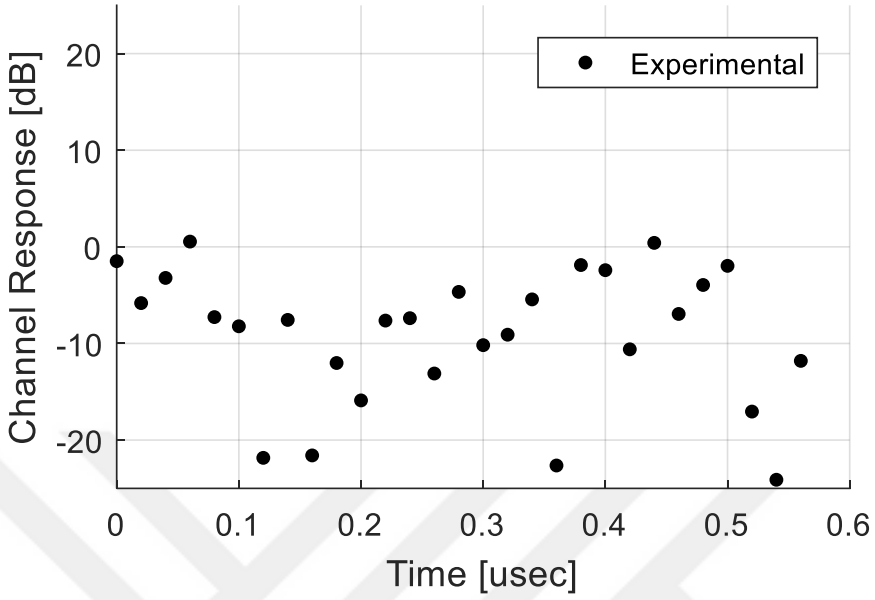

Figure 3.1: Channel response for bandwidth 50 MHz

To hypnotize the model from measurement data, let us consider the general form of Fourier series, which involves *sines* and *cosines*. The values of these *sines* and *cosines* can be obtained as

$$f_1(x) = \cos x \tag{3.10}$$

$$f_2(x) = \sin x \tag{3.11}$$

Which gives us the Fourier series for a function $f_x$as follows

$$f_x = \frac{1}{2}a_o + \sum_{n=1}^{\infty} a_n \cos(nx) + \sum_{n=1}^{\infty} b_n \sin(nx) \tag{3.12}$$

Where

$$a_o = \frac{1}{\pi}\int_{-\pi}^{\pi} f_x \, dx \tag{3.13}$$

$$a_n = \frac{1}{\pi}\int_{-\pi}^{\pi} f_x \cos(nx) \, dx \tag{3.14}$$

$$b_n = \frac{1}{\pi}\int_{-\pi}^{\pi} f_x \sin(nx)\, dx \tag{3.15}$$

The above equations form an orthogonal system for n=1, 2, 3, 4……..

To get the model we need to fit an equation to the collected data. After intensive experiments, it is found that the model must be of the form

$$f_x = a_o + \sum_{n=1}^{\infty} a_n \cos(xw) + \sum_{n=1}^{\infty} b_n \sin(xw) \tag{3.16}$$

Where a_o, a_n, b_n are the coefficients and *w* represents the weighting term. Which is used in the calculation of chi-square. If the value of the standard deviation σ is available, weight can be used as $w=\sigma$ which is necessary to calculate valid error bars of the fit.

To get the desired model starting from eq. (3.16) which actually is a 1 term equation and can be explicitly written as

$$f_x = -134.4 + (-0.5977)\cos(xw) + 5.371 * \sin(xw) \tag{3.17}$$

The details of the extraction of the equations can be found in below sections. All the equations are extracted using MATLAB.

3.12.1 1 Term Model

$$f(x) = a0 + a1 * cos(x * w) + b1 * sin(x * w) \tag{3.18}$$

Coefficients (with 95% confidence bounds):

$a0 = -134.4\ (-136.8, -132)$

$a1 = -0.5977\ (-7.795, 6.6)$

$b1 = 5.371\ (2.033, 8.709)$

$w = 31.1\ (27.68, 35.95)$

Goodness of fit:

SSE: 895.1

R-square: 0.3102

Adjusted R-square: 0.2274

RMSE: 6.174

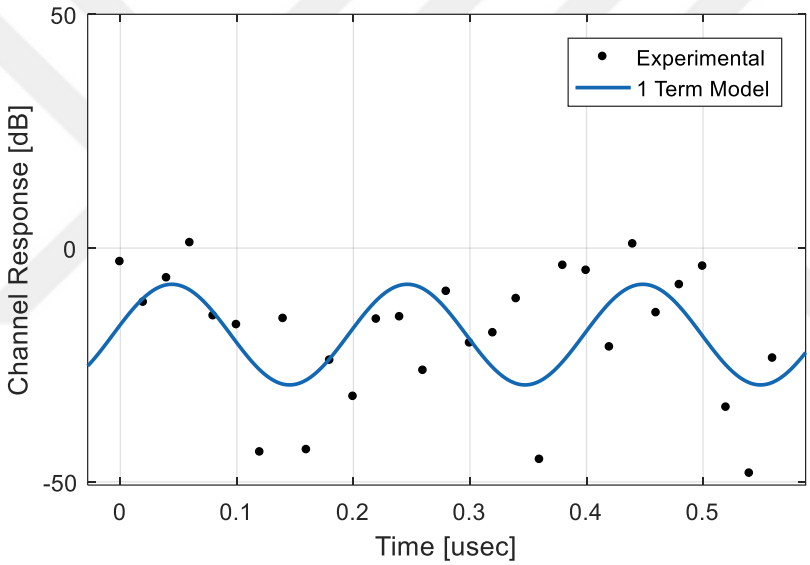

Figure 3.2: Fitted curve using 1 term model

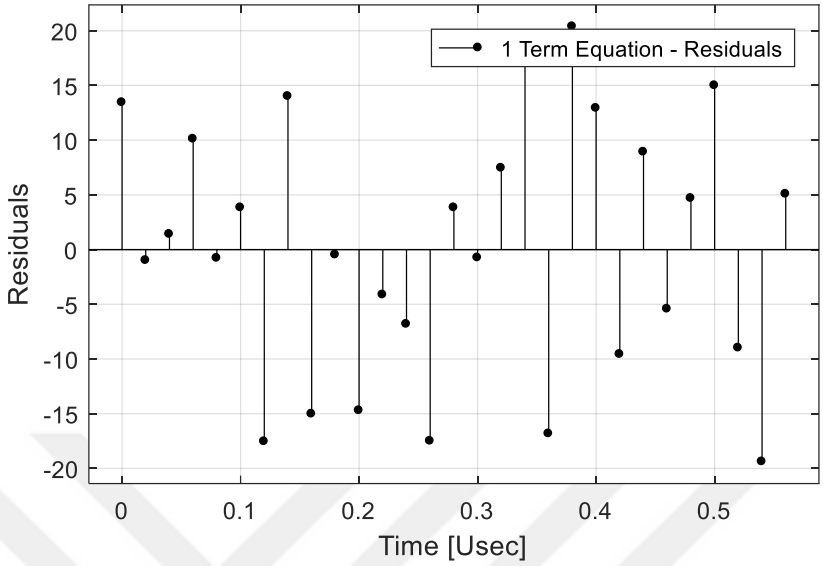

Figure 3.3: 1 term model residual plot

The fitted curved using 1 term equation is shown in Figure 3.2, the results were not at the desired level for which we performed number of experiments to improve the statistical results of the fitted model. The number of terms in the equation are increased by 2, up to 8 terms equations presented in the sub sections of section 3.12.

3.12.2 2 Terms Model

$$f(x) = a0 + a1 * cos(x * w) + b1 * sin(x * w) + a2 * cos(2 * x * w) + b2 * sin(2 * x * w) \quad (3.19)$$

Coefficients (with 95% confidence bounds):

$a0 = -134.5 \ (-136.9, -132.1)$

$a1 = 3.585 \ (0.1046, 7.066)$

$b1 = -0.3411 \ (-4.225, 3.543)$

$a2 = -0.1805 \ (-6.011, 5.65)$

$b2 = 4.517 \ (1.263, 7.772)$

$w = 15.49\ (13.63, 17.35)$

Goodness of fit:

SSE: 740.4

R-square: 0.4524

Adjusted R-square: 0.3333

RMSE: 5.735

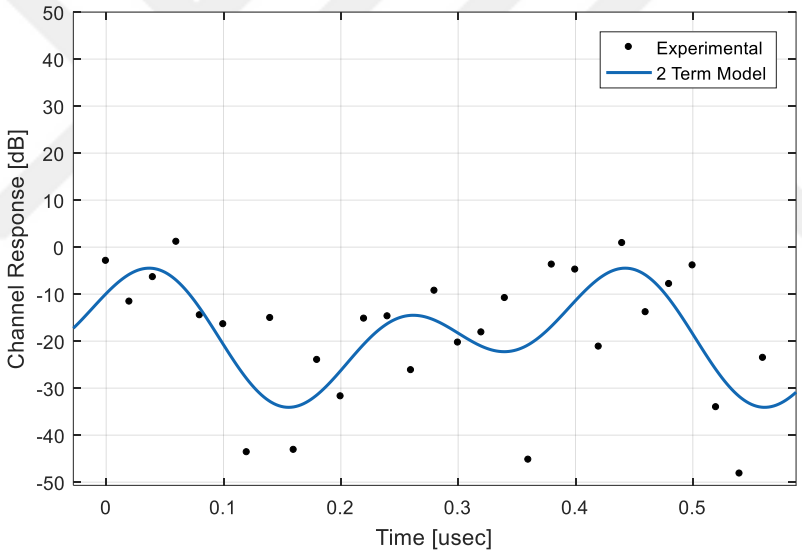

Figure 3.4: Fitted curve using 2 terms model

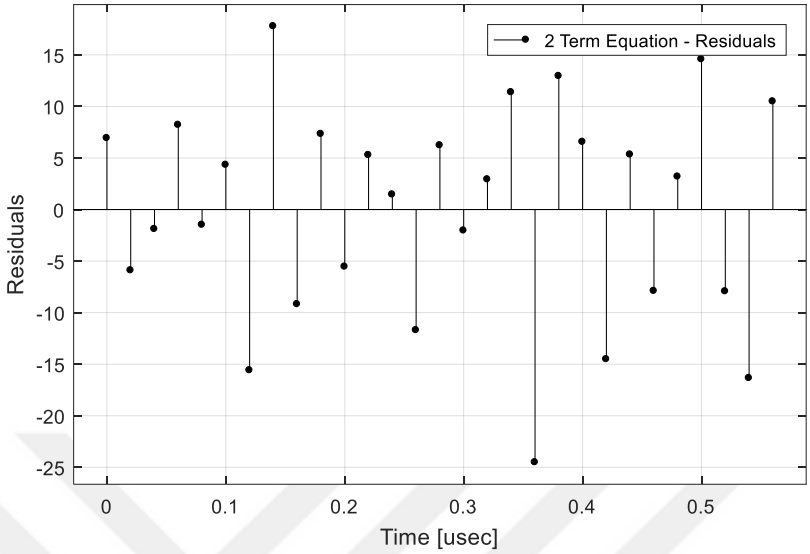

Figure 3.5: 2 terms model residual plot

3.12.3 3 Terms Model

$$f(x) = a0 + a1 * cos(x * w) + b1 * sin(x * w) + a2 * cos(2 * x * w) + b2 * sin(2 * x * w) + a3 * cos(3 * x * w) + b3 * sin(3 * x * w) \quad (3.20)$$

Coefficients (with 95% confidence bounds):

$a0 = -134.4\ (-136.8, -132)$

$a1 = -3.945\ (-7.524, -0.3657)$

$b1 = 2.768\ (-1.149, 6.684)$

$a2 = -3.139\ (-6.672, 0.3934)$

$b2 = 0.7873\ (-3.73, 5.305)$

$a3 = -2.686\ (-6.841, 1.47)$

$b3 = 1.491\ (-3.442, 6.424)$

$w = \quad 15.46 \ (14.33, 16.53)$

Goodness of fit:

SSE: 738.3

R-square: 0.4605

Adjusted R-square: 0.2807

RMSE: 5.958

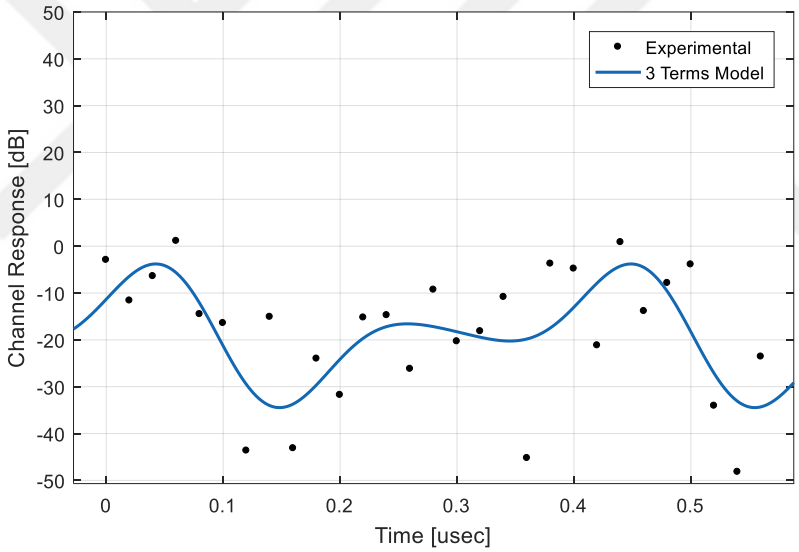

Figure 3.6: Fitted curve using 3 terms model

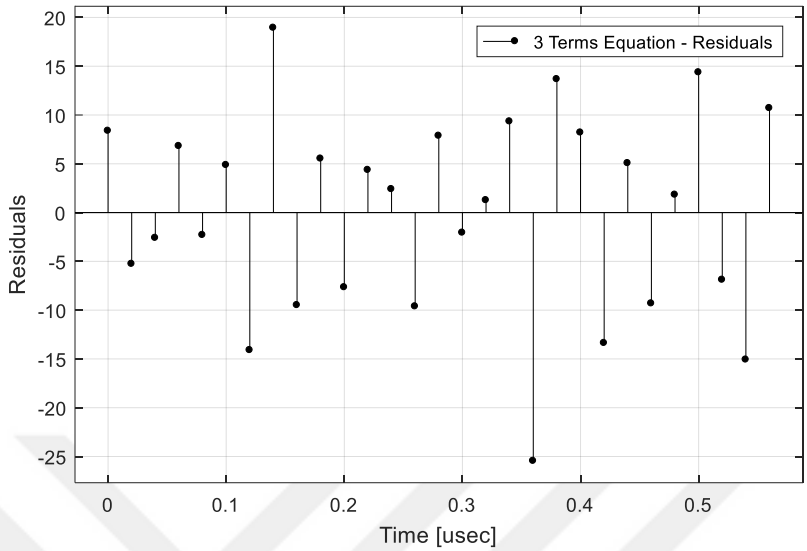

Figure 3.7: 3 terms model residual plot

3.12.4 4 Terms Model

$$f(x) = a0 + a1 * cos(x * w) + b1 * sin(x * w) + a2 * cos(2 * x * w) + b2 * sin(2 * x * w) + a3 * cos(3 * x * w) + b3 * sin(3 * x * w) + a4 * cos(4 * x * w) + b4 * sin(4 * x * w) \quad (3.21)$$

Coefficients (with 95% confidence bounds):

$a0 = -134.2 \ (-136.7, -131.8)$

$a1 = -2.04 \ (-6.284, 2.205)$

$b1 = 4.842 \ (1.331, 8.353)$

$a2 = 0.6104 \ (-3.571, 4.792)$

$b2 = 1.994 \ (-1.466, 5.454)$

$a3 = \quad 1.84 \ (-2.182, 5.861)$

$b3 = \quad 1.116 \ (-2.962, 5.194)$

$a4 = \quad 3.155 \ (-0.4633, 6.773)$

$b4 = \quad 0.5592 \ (-5.417, 6.535)$

$w = \quad 8.450 \ (8.24, 8.77)$

Goodness of fit:

SSE: 678.2

R-square: 0.5279

Adjusted R-square: 0.3043

RMSE: 5.858

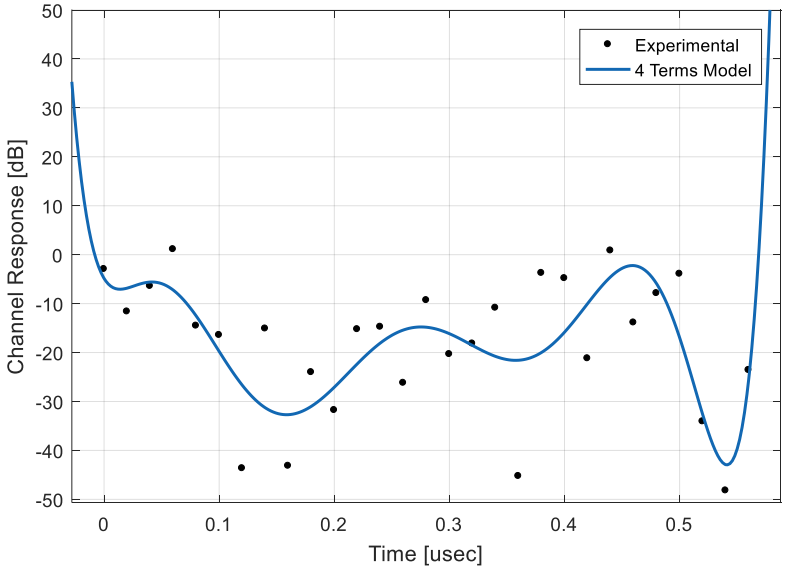

Figure 3.8: Fitted curve using 4 terms model

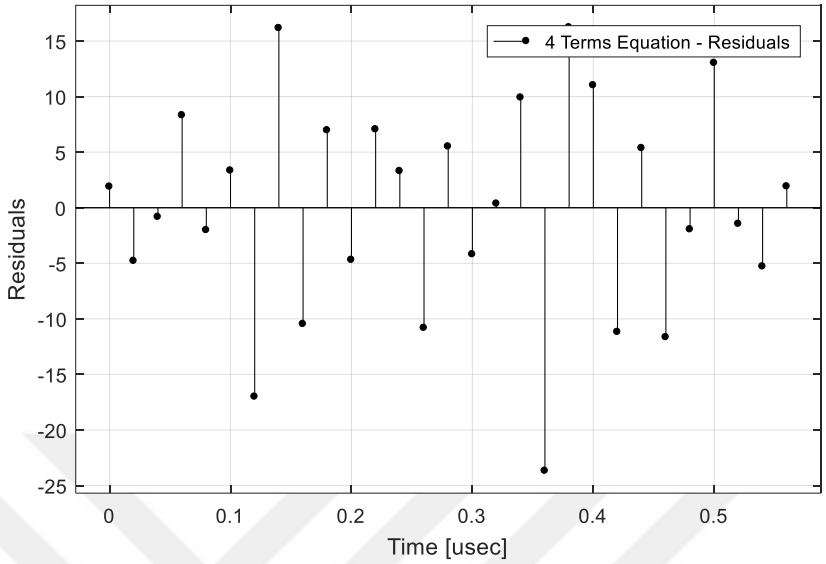

Figure 3.9: 4 terms model residual plot

3.12.5 5 Terms Model

$$f(x) = a0 + a1 * cos(x * w) + b1 * sin(x * w) + a2 * cos(2 * x * w) + b2 * sin(2 * x * w) + a3 * cos(3 * x * w) + b3 * sin(3 * x * w) + a4 * cos(4 * x * w) + b4 * sin(4 * x * w) + a5 * cos(5 * x * w) + b5 * sin(5 * x * w) \quad (3.22)$$

Coefficients (with 95% confidence bounds):

$a0 = -134.3 \ (-136.8, -131.9)$

$a1 = -3.882 \ (-7.553, -0.2114)$

$b1 = 2.824 \ (-1.146, 6.794)$

$a2 = -3.072 \ (-6.742, 0.597)$

$b2 = 0.9167\ (-3.646, 5.479)$

$a3 = -2.701\ (-7.433, 2.032)$

$b3 = 1.803\ (-3.266, 6.872)$

$a4 = -6.373\ (-66.5, 53.76)$

$b4 = 6.502\ (-19.68, 32.68)$

$a5 = 9.389\ (-50.18, 68.96)$

$b5 = 0.01993\ (-24.27, 24.31)$

$w = 6.732\ (5.97, 7.93)$

Goodness of fit:

SSE: 592.5

R-square: 0.5642

Adjusted R-square: 0.2822

RMSE: 5.951

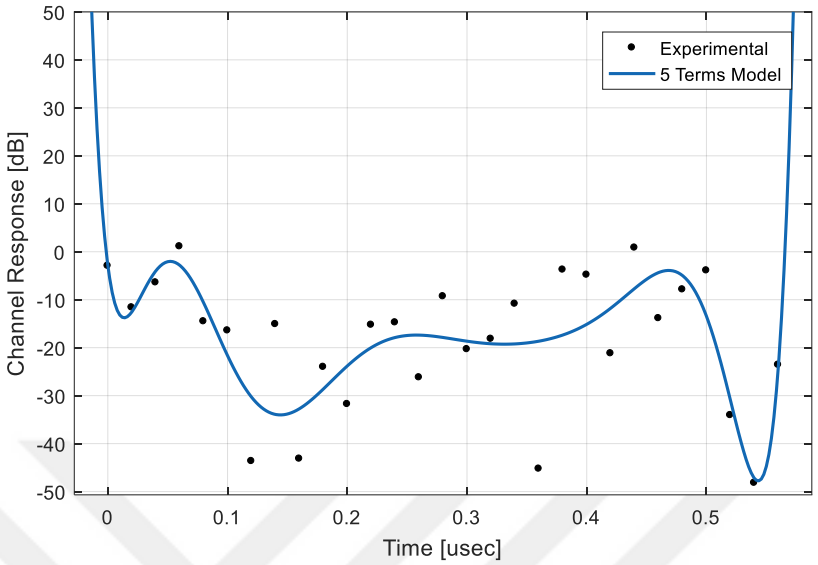

Figure 3.10: Fitted curve using 5 terms model

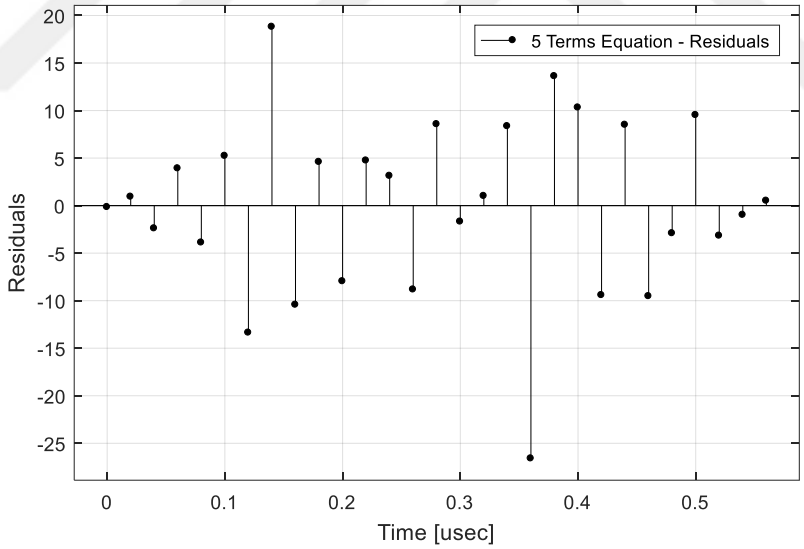

Figure 3.11: 5 terms model residual plot

3.12.6 6 Terms Model

$$f(x) = a0 + a1 * cos(x * w) + b1 * sin(x * w) + a2 * cos(2 * x * w) + b2 * sin(2 * x * w) + a3 * cos(3 * x * w) + b3 * sin(3 * x * w) + a4 * cos(4 * x * w) + b4 * sin(4 * x * w) + a5 * cos(5 * x * w) + b5 * sin(5 * x * w) + a6 * cos(6 * x * w) + b6 * sin(6 * x * w) \quad (3.23)$$

Coefficients (with 95% confidence bounds):

$a0 = -134.4\ (-136.7, -132.1)$

$a1 = -2.214\ (-5.646, 1.217)$

$b1 = 4.937\ (1.721, 8.152)$

$a2 = 0.3947\ (-3.035, 3.824)$

$b2 = 1.921\ (-1.311, 5.152)$

$a3 = 1.025\ (-2.54, 4.59)$

$b3 = 1.08\ (-2.38, 4.54)$

$a4 = 3.52\ (0.01519, 7.024)$

$b4 = -0.0001037\ (-4.41, 4.41)$

$a5 = -0.1046\ (-4.217, 4.008)$

$b5 = -2.061\ (-5.599, 1.477)$

$a6 = -0.07625\ (-5.462, 5.309)$

$b6 = -3.794\ (-7.244, -0.3433)$

$w = 32.92\ (32.33, 33.51)$

Goodness of fit:

SSE: 446

R-square: 0.6664

Adjusted R-square: 0.3774

RMSE: 5.543

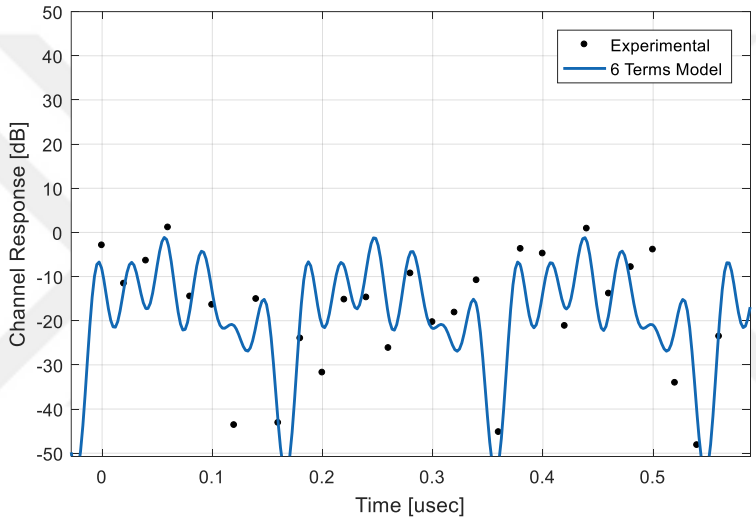

Figure 3.12: Fitted curve using 6 terms model

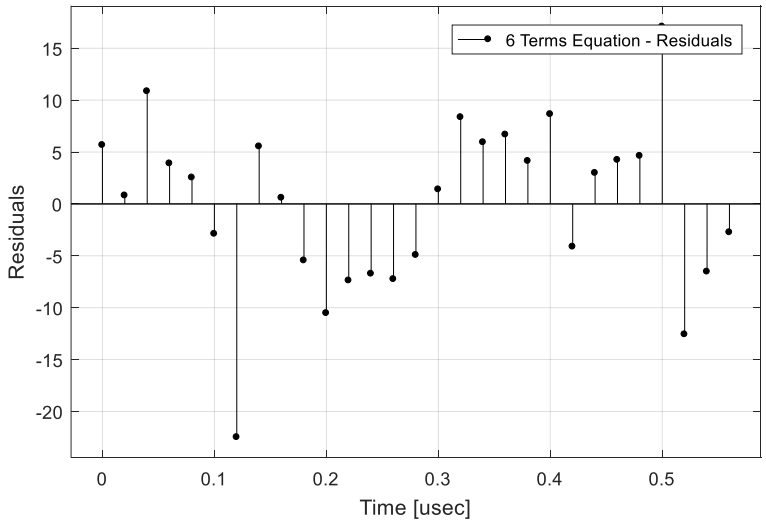

Figure 3.13: 6 terms model residual plot

3.12.7 7 Terms Model

$$f(x) = a0 + a1 * cos(x * w) + b1 * sin(x * w) + a2 * cos(2 * x * w) + b2 * sin(2 * x * w) + a3 * cos(3 * x * w) + b3 * sin(3 * x * w) + a4 * cos(4 * x * w) + b4 * sin(4 * x * w) + a5 * cos(5 * x * w) + b5 * sin(5 * x * w) + a6 * cos(6 * x * w) + b6 * sin(6 * x * w) + a7 * cos(7 * x * w) + b7 * sin(7 * x * w) \quad (3.24)$$

Coefficients (with 95% confidence bounds):

$a0 = -134.4 \ (-137.1, -131.7)$

$a1 = 2.646 \ (-1.098, 6.389)$

$b1 = 1.254 \ (-2.645, 5.153)$

$a2 = -3.521 \ (-7.314, 0.2725)$

$b2 = 1.68 \ (-2.321, 5.682)$

$a3 = -0.3512 \ (-4.212, 3.509)$

$b3 = -0.05441 \ (-3.812, 3.703)$

$a4 = -3.202 \ (-7.073, 0.6684)$

$b4 = 0.09886 \ (-4.2, 4.398)$

$a5 = 0.4883 \ (-3.39, 4.366)$

$b5 = -0.1135 \ (-3.942, 3.716)$

$a6 = -3.067 \ (-6.879, 0.7452)$

$b6 = -0.1407 \ (-4.985, 4.704)$

$a7 = -3.102 \ (-7.202, 0.9972)$

$b7 = \quad -1.63 \ (-6.536, 3.275)$

$w = \quad 33.12 \ (32.23, 34.12)$

Goodness of fit:

SSE: 455.6

R-square: 0.6725

Adjusted R-square: 0.2946

RMSE: 5.90

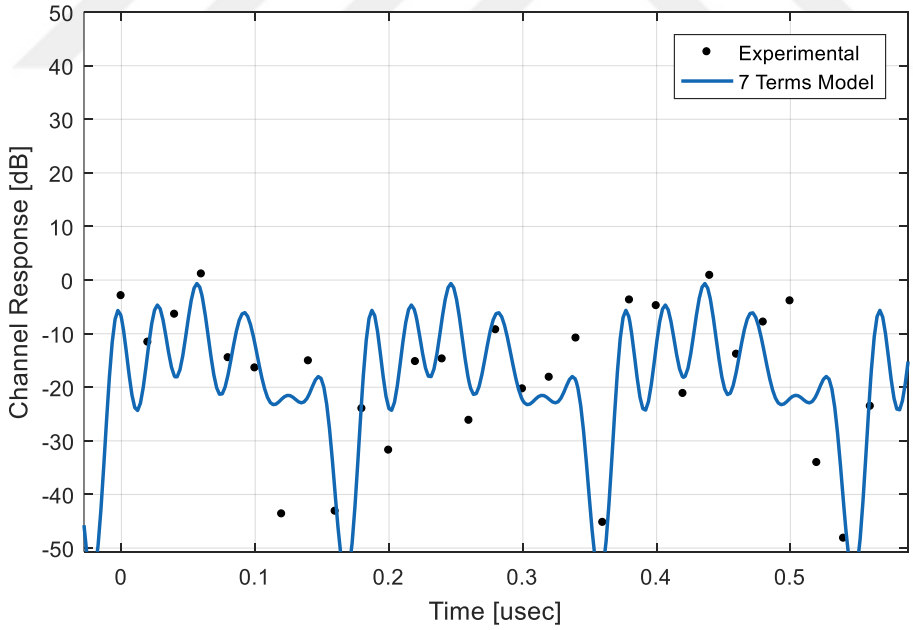

Figure 3.14: Fitted curve using 7 terms model

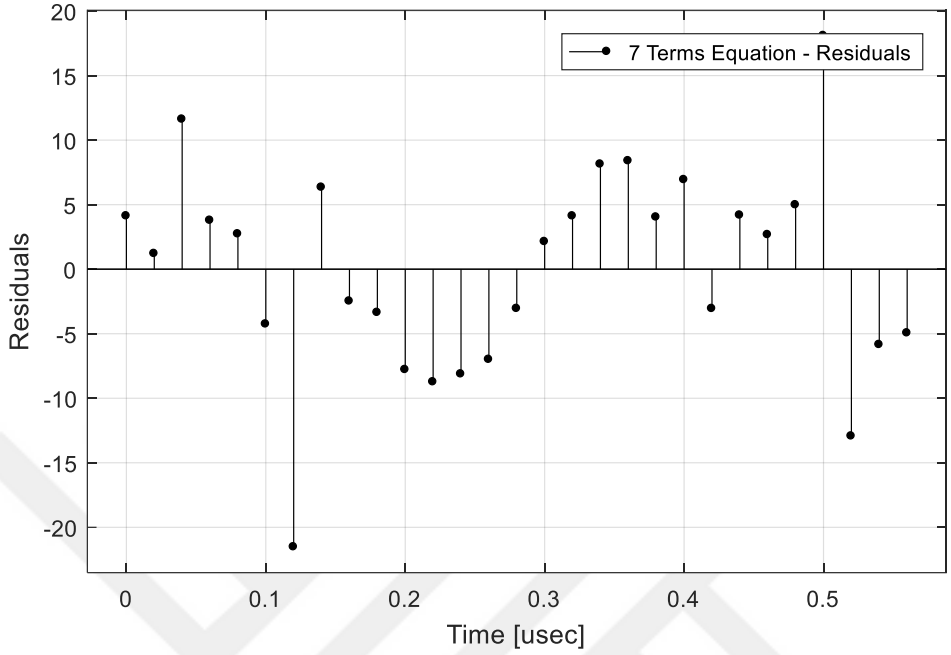

Figure 3.15: 7 terms model residual plot

3.12.8 8 Terms Model (Proposed Model)

$$f(x) = a0 + a1 * cos(x * w) + b1 * sin(x * w) + a2 * cos(2 * x * w) + b2 * sin(2 * x * w) + a3 * cos(3 * x * w) + b3 * sin(3 * x * w) + a4 * cos(4 * x * w) + b4 * sin(4 * x * w) + a5 * cos(5 * x * w) + b5 * sin(5 * x * w) + a6 * cos(6 * x * w) + b6 * sin(6 * x * w) + a7 * cos(7 * x * w) + b7 * sin(7 * x * w) + a8 * cos(8 * x * w) + b8 * sin(8 * x * w) \quad (3.25)$$

Coefficients (with 95% confidence bounds):

$a0 = \quad -9.382 \ (-11.68, -7.085)$

$a1 = \quad 3.984 \ (0.67, 7.298)$

$b1 = \quad -0.5262 \ (-3.785, 2.733)$

$a2 = \quad 0.7176 \ (-2.891, 4.326)$

$b2 = \quad 4.324 \ (1.063, 7.584)$

$a3 = \quad -0.5402 \ (-3.811, 2.73)$

$b3 = \quad 0.4261 \ (-2.851, 3.703)$

$a4 = \quad 1.292 \ (-1.911, 4.495)$

$b4 = \quad -0.8812 \ (-4.37, 2.607)$

$a5 = \quad 2.254 \ (-1.059, 5.567)$

$b5 = \quad -1.53(-5.438, 2.378)$

$a6 = \quad 0.2745 \ (-2.96, 3.509)$

$b6 = \quad -0.2933 \ (-3.619, 3.032)$

$a7 = \quad -0.1391 \ (-4.928, 4.649)$

$b7 = \quad -3.488 \ (-6.72, -0.2568)$

$a8 = \quad -1.608 \ (-6.193, 2.976)$

$b8 = \quad -2.977 \ (-6.533, 0.5796)$

$w = \quad 15.24 \ (14.72, 15.76)$

Goodness of fit:

SSE: 291.4

R-square: 0.7766

Adjusted R-square: 0.4312

RMSE: 5.297

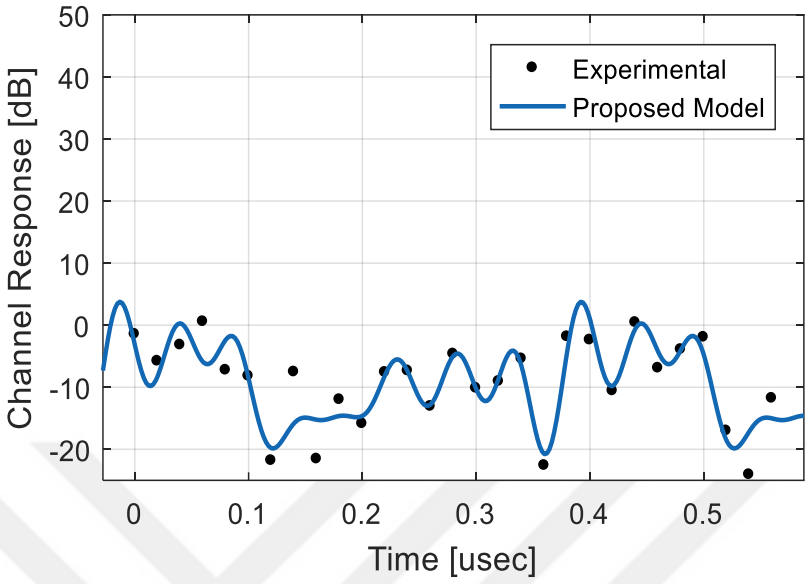

Figure 3.16: Fitted curve using 8 terms proposed model

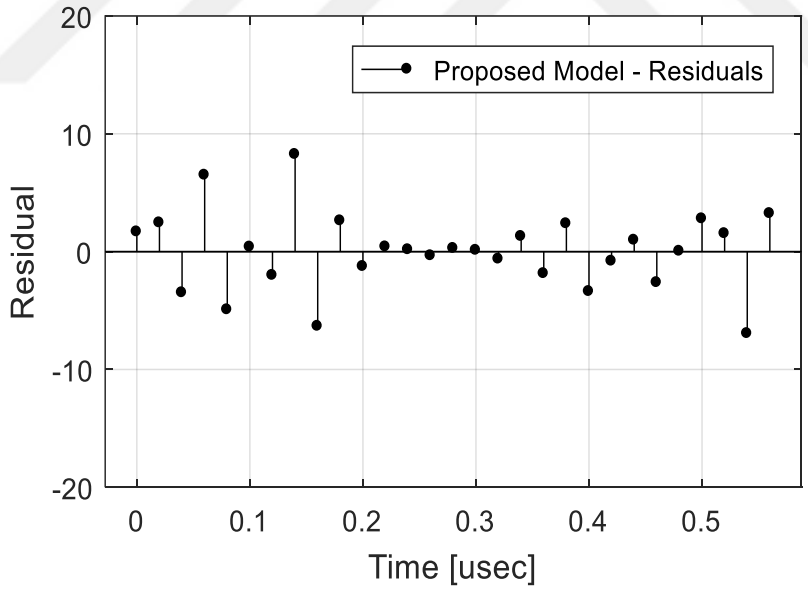

Figure 3.17: 8 terms proposed model residual plot

It is observed that if we proceed by increasing number of terms for the equations, the mathematical complexity is increasing without any significant amount of accuracy for the fit, so we decided to stop with the 8 terms equation, the final proposed eq. (3.26) results in the highest RMSE = 5.297. Figure 3.16 show the final proposed model concerning the experimental data.

Finally Figure 3.17 present the residual plot with the leftovers of the subtracted fit from the experimental data. The fitting statistics for all those experiments are shown in Table 3.1.

Table 3.1: Fitted statistics results

No of Terms	R-Squared	Adjusted R-Squared	RMSE	Weights
1 Term Equation	0.3102	0.2274	6.174	31.1
2 Terms Equation	0.4524	0.3333	5.735	15.49
3 Terms Equation	0.4605	0.2807	5.958	15.46
4 Terms Equation	0.5279	0.3043	5.858	8.450
5 Terms Equation	0.5642	0.2822	5.951	6.732
6 Terms Equation	0.6664	0.3774	5.543	32.92
7 Terms Equation	0.6725	0.2946	5.90	33.12
8 Terms Proposed Model	0.7766	0.4312	5.297	15.24

$$f_x = -9.382 + 3.984 * \cos(x * 15.24) + (-0.5262) * \sin(x * 15.24) + 0.7176 * \cos(2 * x * 15.24) + 4.324 * \sin(2 * x * 15.24) + (-0.5402) * \cos(3 * x * 15.24) + 0.4261 * \sin(3 * x * 15.24) + 1.292 * \cos(4 * x * 15.24) + (-0.8812) * \sin(4 * x * 15.24) + 2.254 * \cos(5 * x * 15.24) + (-1.53) * \sin(5 * x * 15.24) + 0.2745 * \cos(6 * x * 15.24) + (-0.2933) * \sin(6 * x * 15.24) + (-0.1391) * \cos(7 * x * 15.24) + (-3.488) * \sin(7 * x * 15.24) + (-1.608) * \cos(8 * x * 15.24) + (-2.977) * \sin(8 * x * 15.24) \quad (3.26)$$

Generally eq. (3.26) can be written as eq. (3.27)

$$f_x = a_o + a_1 * \cos(x * w) + b_1 * \sin(x * w) + a_2 * \cos(2 * x * w) + b_2 * \sin(2 * x * w) + a_3 * \cos(3 * x * w) + b_3 * \sin(3 * x * w) + \quad (3.27)$$

Or eq. (3.28)

$$f_x = a_o + \sum_{n=1}^{8} a_n \cos(n * x * w) + \sum_{n=1}^{8} b_n \sin(n * x * w) \quad (3.28)$$

95% confidence limits for each coefficient of the proposed model can be found in Table 3.2. The confidence limits means that the estimate of the parameter lies between $\pm\delta$ with a 95% probability.

Table 3.2: 95 % Confidence Limits

Coefficient		95% Confidence Limits	
a_o		(-11.68, -7.085)	
a_n	Limits	b_n	Limits
a_1	(0.67, 7.298)	b_1	(-3.785, 2.733)
a_2	(-2.891, 4.326)	b_2	(1.063, 7.584)
a_3	(-3.811, 2.73)	b_3	(-2.851, 3.703)
a_4	(-1.911, 4.495)	b_4	(-4.37, 2.607)
a_5	(-1.059, 5.567)	b_5	(-5.438, 2.378)
a_6	(-2.96, 3.509)	b_6	(-3.619, 3.032)
a_7	(-4.928, 4.649)	b_7	(-6.72, -0.2568)
a_8	(-6.193, 2.976)	b_8	(-6.533, 0.5796)

Using eq. (3.26) we are able to get the best possible Fit for the experimental data, besides that by observing Table 3.1 it can be seen that we can also get reasonable RMSE values with 2 Terms and 6 Terms equations. These equations can be extracted from eq. (3.26) just by reducing the no of terms to get the desired results. We used the 8 Terms equation to get the best results although from those experiments it is clear that there is a tradeoff between mathematical complexity and accuracy of the fit depending on the requirements one can easily select between 2 Terms, 6 Terms or 8 Terms equation according to the requirements.

3.13 BLIND TESTING

To check the success rate of the mathematical model, a blind test was conducted. The data has not been used in fitting data. A new channel response was selected for this test, the experiment was performed using the proposed model against the new channel response data. Figure 3.18 shows the comparison of the fitted model using the proposed model for new data. Figure 3.19 shows the prediction error of blind channel response data (i.e., data which was not used in fitting and derivation process of the proposed mathematical model) in the form of residual plot and is given as RMSE 7.76. This all indicates the high accuracy of the proposed model as compared with the experimental data from the simulation.

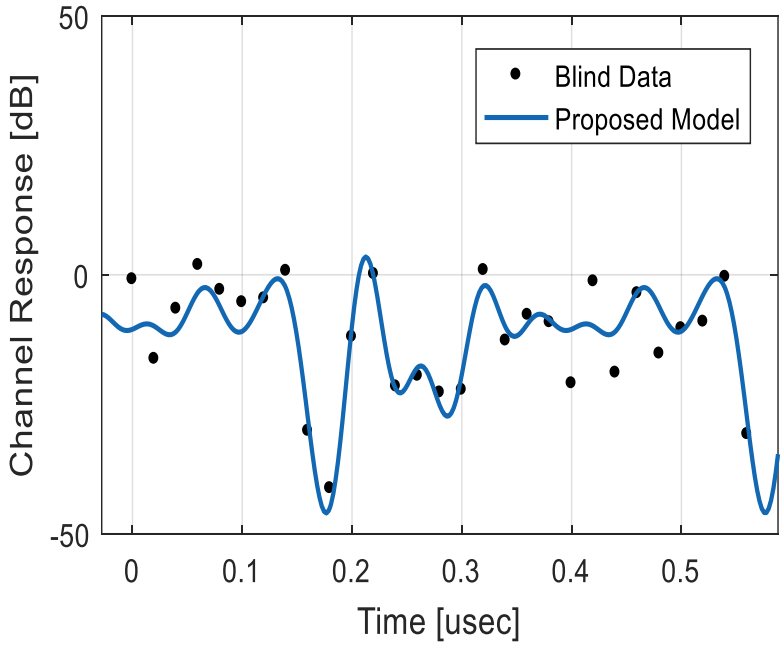

Figure 3.18: Fitted curve using proposed model vs blind data

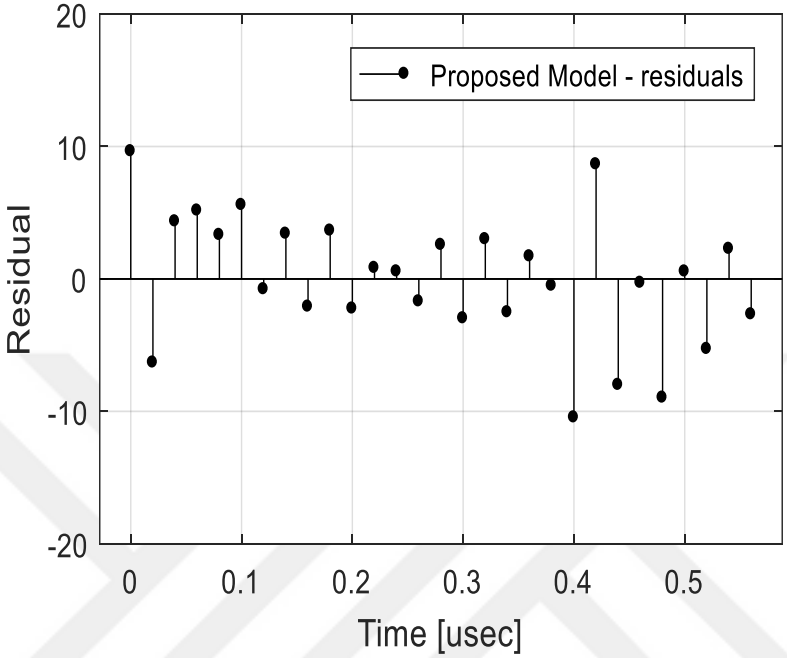

Figure 3.19: Residual plot of blind data vs proposed model

4 EQUALIZATION AND SYSTEM PERFORMANCE

Wireless communication systems consist of transmitter, channel and receiver with additional steps as shown in Figure 4.1. Although there are number of steps involved and can be added according to the channel conditions to improve the communication system. The transmitter transmits the data through the channel. Channel is considering as a black box as no one can exactly know what is happening inside the channel it is highly predictable and can be change according to the conditions and environment. The receiver task is to receive the data and extract the information transmitted by the transmitter but there is always missing information called bit errors. Those are the missing bits or bits with errors which were not as the original bits transmitted from the transmitter. There are number of techniques used to improve the Bit Error Rate (BER). There are some channel estimation techniques, channel coding, diversity equalization etc. Each technique is used according to the system, equalizers are normally used to overcome the problem of Inter-Symbol Interference (ISI) created by multipath, channel coding is used to improve the link performance of the small-scale b adding the redundant data bits in the transmitted message. A brief introduction is presented in the upcoming sections to help understand the results and the process of finding them.

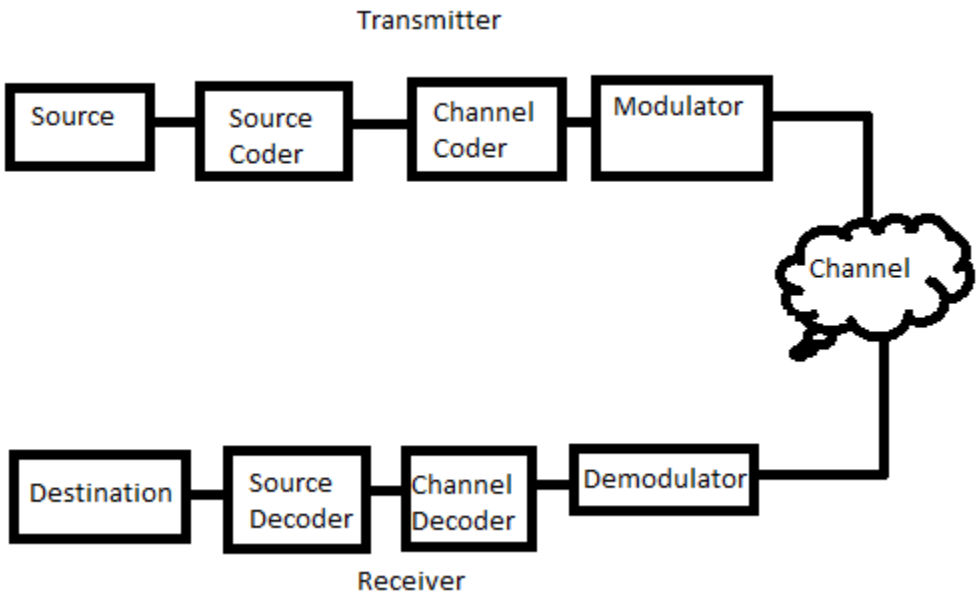

Figure 4.1: Wireless communication block diagram

4.1 ULTRA-WIDEBAND

Ultra-Wide Band (UWB) is a wireless communication system used in different wireless networks using low power and high bandwidths. The UWB technology is a perfect choice by the consumers and engineers working in a short range environment for high data speeds using high bandwidths with low power consumptions over a wide spectrum of frequency bands. Figure 4.2 presents the comparison of 2G, 3G, wireless Local Area Network (LAN) and UWB.

There are two main applications of ultra-wide band as below:

The first one is the radar communication in which the signals penetrate the nearby surface but reflects back from the surfaces that are further away, which allow objects to be detected even if behind the walls.

The second application is voice and data transmission using digital pulses, by allowing low powered but extremely high data rates with in a specific range.

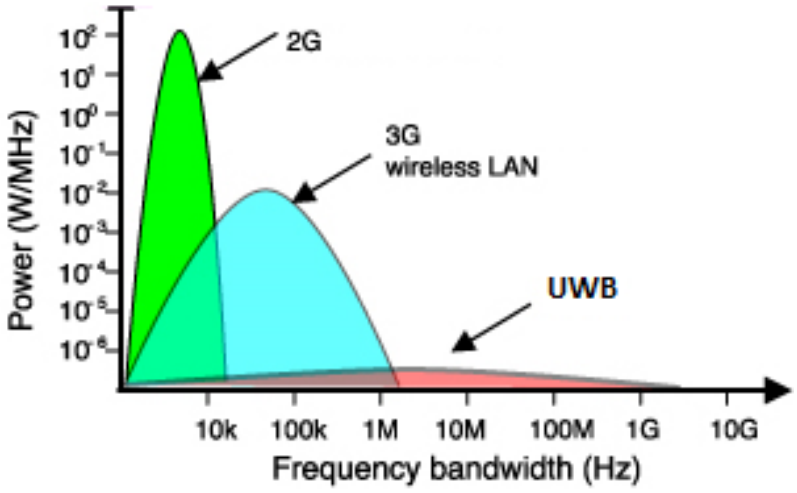

Figure 4.2: Ultra-wide band

4.2 COHERENCE BANDWIDTH

Coherence bandwidth is a statistical measurement of the range of frequencies over which the channel can be considered as flat, or the frequency interval over which the two frequencies of a signal are likely to experience comparable amplitude fading. By flat we mean a channel which passes all spectral components with approximately equal gain and linear phase. If the coherence bandwidth is define as the bandwidth over which the frequency correlation function is above 0.9, then the coherence bandwidth is approximately presented as eq. (4.1).

$$B_c \approx \frac{1}{50\sigma_\tau} \tag{4.1}$$

If the definition is relaxed so that the frequency correlation function is above 0.5, then the coherence bandwidth is approximately equal to eq. (4.2)

$$B_c \approx \frac{1}{5\sigma_\tau} \tag{4.2}$$

4.3 BIT ERROR RATE

Bit Error Rate (BER) in digital communication can be define as the number of received bits of a data stream over a communication channel that have been altered due to noise fading multipath or any other reason. It can be also define as the number of bit errors per unit time. We can calculate the BER if we can divide the number of bit errors by the total number of transmitted bits during a specific time interval.

$$BER = \frac{Number\ of\ errors}{Total\ number\ of\ bits\ sent}$$

Bit error rate can be calculated for any communication system using different equations to calculate the bit errors. For example, in the case of Quadrature Phase Shift Keying (QPSK)

modulation and Additive White Gaussian Noise (AWGN) channel, the BER of the Eb/No is given by eq. (4.3)

$$BER = \frac{1}{2} erfc\left(\sqrt{Eb/No}\right) \tag{4.3}$$

Erf, is the error function.

Eb, is the energy in 1 bit.

No, is the noise power spectral density (which is the noise power in a 1 Hz bandwidth)

It should be noted that different types of modulation techniques have their own values for the error function as each type of modulation performs differently in the presence of noise. The Figure 4.3 show the standard BER plot for different modulation schemes.

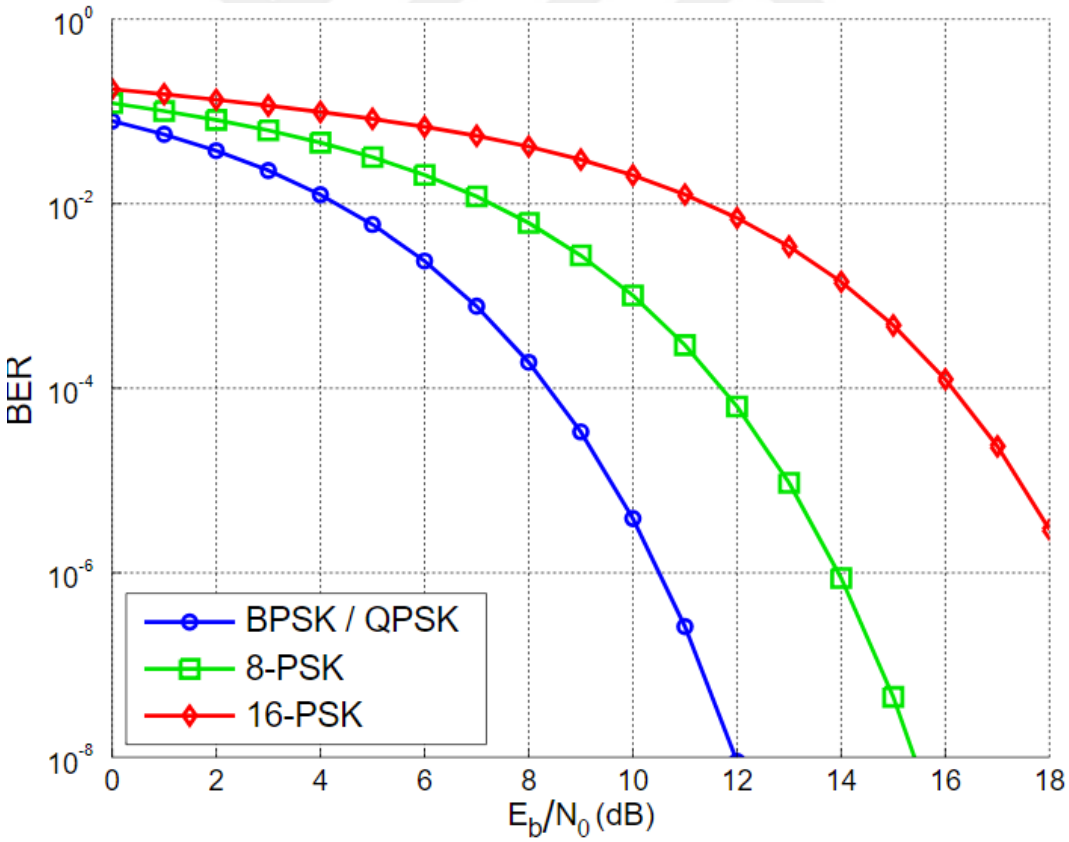

Figure 4.3: BER comparison of different modulation schemes

4.4 CHANNEL ESTIMATION

In wireless communication, there are some known channel properties of a communication link which include how a signal propagates from the transmitter through channel towards the receiver for example fading, scattering and power decay with distance those known channel properties technically known as Channel State Information (CSI) so calculation of CSI for a specific channel by using the known information is called channel estimation. The CSI is estimated at the receiver end of the system and provide feedback to the transmitter that's why transmitter and receiver have different CSI and can be represented as CSIT and CSIR.

For a narrow band flat fading channel with multiple transmitters and multiple receivers the system can be modeled as eq. (4.4)

$$y = Hx + n \tag{4.4}$$

Here y and x are the receive and transmit vectors.

H and n are the channel matrix and noise vector.

4.5 CHANNEL MODELING

It is the mathematical representation of the effect of a channel through which a wireless signal is propagated. The channel model is the impulse response of the channel in time domain or its Fourier transform in the frequency domain. Generally, the channel impulse response of a wireless system varies randomly over time.

Using the right channel model in a design helps optimize the link performance, system architecture tradeoff and provide a realistic assessment of overall system performance.

There are number of parameters involve and need to be consider while designing a new channel model some of the main parameters used in the model can be channel bandwidth, carrier frequency, Doppler frequency, fading etc.

Consider a channel with impulse response h(t) between transmitter and receiver antenna. The transmitted signal x(t) can also be considered as a corrupted signal by additive white Gaussian noise component represented by n(t).

The received signal y(t) can be extracted by the convolution of h(t) and x(t) added with the noise component n(t) as shown in eq. (4.5)

$$y(t) = x(t) \circledast h(t) + n(t) \tag{4.5}$$

While in frequency domain the convolution operations become multiplication as eq. (4.6)

$$Y(f) = X(f)H(f) + N(f) \tag{4.6}$$

4.6 CHANNEL CODING

Channel coding are used to improve the small scale link performance by adding the redundant data bits in the transmitted message to recover the data from the receiver even if an instantons fade occurs in the channel. At the baseband portion of the transmitter the additional bits are added in the message by mapping it to the new message sequence and the new sequence has more bits than the original message and that message is modulated for the transmission in wireless channel.

Channel coding is used in the receiver end to correct part of the message or all the bits with in the message introduced by the channel. As decoding is performed after the demodulation at the receiver end so coding can be considered as a post detection technique.

There are three main types of channel codes, Block codes, convolutional codes and Turbo codes.

Channel coding protects digital data from errors by selectively introducing redundancies in the transmitted data. Channel codes that are used to detect errors are called error detection codes and codes which can also help correct the errors are called error correction codes.

4.7 INTER-SYMBOL INTERFERENCE

In a communication system data is transmitted as ones and zeros and can be represented as Figure 4.4 showing the rectangular pulses with finite duration τ. While the frequency domain of a rectangular pulse is a sinc function of an infinite duration with maximum energy between -π

and +π as shown in Figure 4.5. This implies a pulse of duration τ requires twice its bandwidth for reliable transmission. For band limited signals in order to increase the data rate we have to increase the number of pulses transmitted per second which will result in the decrease of symbol duration τ and will indicates increase in the frequency requirement that is bandwidth increases, if the channel is band limited that increase can results in overlapping with the neighboring channels results in inter-symbol interference as shown in Figure 4.6.

There are number of techniques used to mitigate the effect of ISI. Equalizers used to compensate for ISI created by multipath within time dispersive channels. The process of using equalizers to compensate the ISI is called equalization. The equalization process and different techniques are discussed in detailed in the next section.

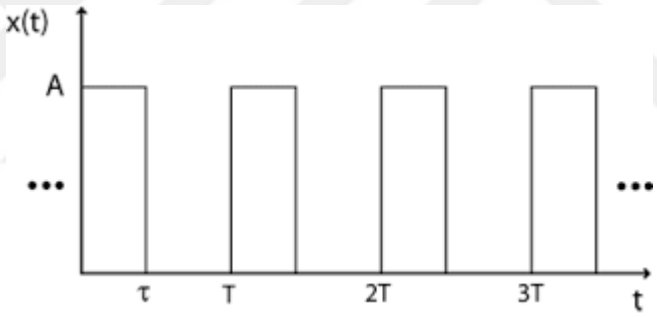

Figure 4.4: Rectangular representation

Figure 4.5: Sinc function

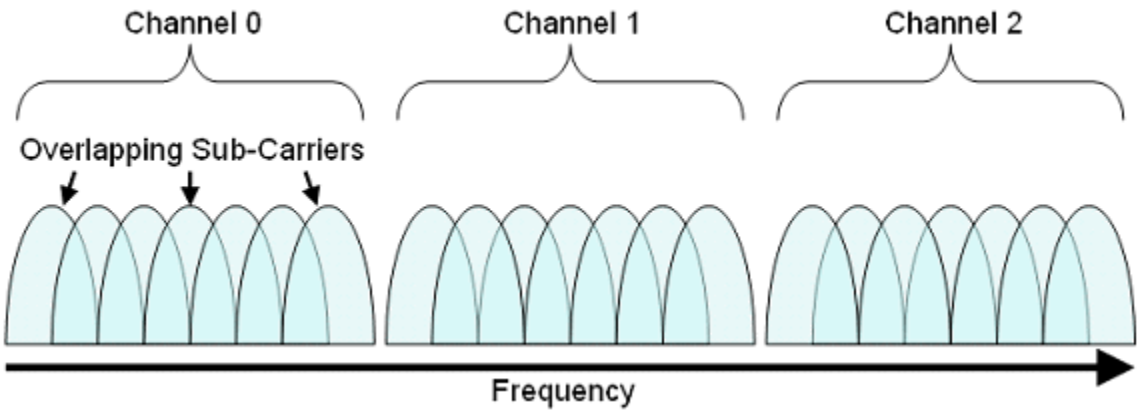

Figure 4.6: Overlapping sub-carriers introducing ISI

4.8 EQUALIZATION

Equalization is the process used in wireless communication to compensate the effect of ISI caused by multipath in time dispersive channels. ISI occurs if the modulation bandwidth exceeds the coherence bandwidth of the radio channel and the pulses are spread in to adjacent symbols. An equalizer with in the receiver can compensate ISI but the equalizer must be adaptive as the channel is normally un predictable and varies with time. ISI caused by multipath bandlimited (frequency selective) time dispersive channels distorts the transmitted signals results in bit errors at the receiver effecting the communication. Adaptive equalizers are used to combat the ISI as the channel is varying with time. The equalizers must act according to the variations of the channel with time to achieve the desired results.

The adaptive equalizers operations can be mainly divided into two parts, training and tracking. Initially, a known training fixed length sequence is sent by the transmitter so that equalizer can train itself in order to improve the BER performance. Following up by the training sequence the user data is sent to evaluate the channel and estimate channel coefficients which can be used to compensate the distortion caused by multipath. The block diagram of an adaptive equalizer can be seen in Figure 4.8 [4].

Equalizers can be mainly divided into two parts linear and nonlinear which are sub divided into multiple section.

Linear equalizers can mainly classify as Transversal and lattice.

Nonlinear equalizers can be mainly classified as DFE, ML symbol detector and MLSE.

Transversal contains zero forcing, LMS and RLS equalizers while lattice contains Gradient RLS as shown in Figure 4.7. Each equalizer has their own properties and can be used accordingly. For example, the recursive least square equalizers converge quickly as compare to the least mean square equalizer, while on the other hand LMS can execute quickly as compare to the RLS but it takes time to converge. These equalizers can also be used in combination by exploiting their properties. Although from experiments it is clear that in most of the cases nonlinear equalizers will outperform the linear equalizers in performance and will results n better BER performance as compare to the counter party linear equalizers.

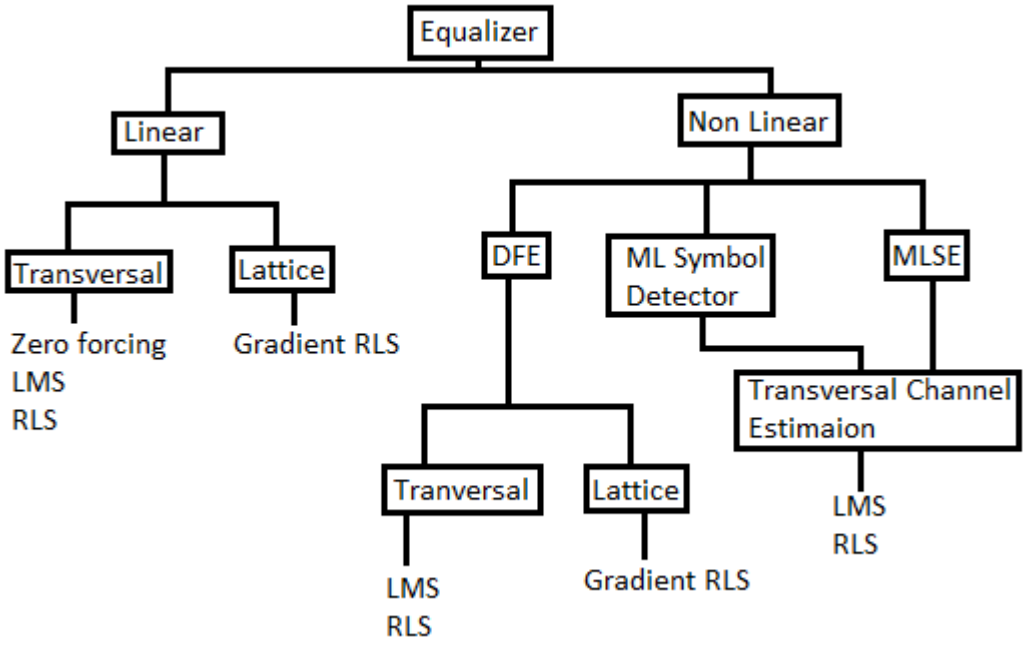

Figure 4.7: Equalizers types and classification

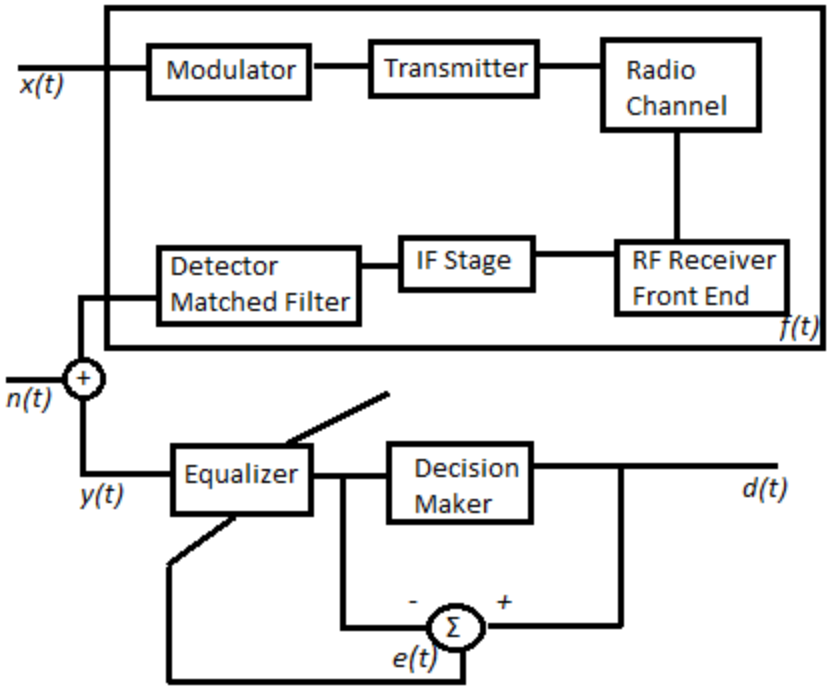

Figure 4.8: Block diagram of an adaptive equalizer at the receiver

4.9 RECURSIVE LEAST SQUARE

Recursive least square is an equalizer used to finds the coefficients related to the input signal. The main advantage of RLS is it converges really quickly but the disadvantage is its mathematical complexity.

Suppose that a signal *d(n)* is transmitted through a noisy channel and the received signal is eq. (4.7)

$$x(n) = \sum_{k=0}^{q} b_n(k)\, d(n-k) + v(n) \tag{4.7}$$

Where *v(n)* represents additive noise, *d(n)* is our desired signal

$$d(n) \approx \sum_{k=0}^{p} w(k)\, x(n-k) = W^T X_n \tag{4.8}$$

Where

$$X(n) = [x(n) \quad x(n-1) \quad \ldots\ldots \quad x(n-p)]^T \tag{4.9}$$

Which is the column vector containing *p+1* most recent samples of *x(n)*. The estimate of the recovered desired signal can have represented as eq. (4.10)

$$\hat{d}(n) = \sum_{k=0}^{p} w_n(k)x(n-k) = W_n^T X_n \tag{4.10}$$

We need to estimate the parameter *W* at each time n which is currently presented as W_n and is a column vector while its transpose W_n^T is a row vector. While the product $W_n^T X_n$ is actually the dot product of W_n and X_n which is equal to $\hat{d}(n)$ which itself is a scaler. The feedback diagram of RLS can be seen in Figure 4.9.

Where *e(n)* represent the error signal and *d(n)* represent the desired signal. The error depends on filter coefficients through $\hat{d}(n)$.

$$e(n) = d(n) - \hat{d}(n) \tag{4.11}$$

While the cost function we desired to minimize

$$C(W_n) = \sum_{i=0}^{n} \lambda^{n-i} e^2(i) \tag{4.12}$$

Where $0 < \lambda \leq 1$, we can minimize the function by taking derivatives of the cost function and setting the result to zero.

$$\frac{dC(W_n)}{dw_n(k)} = \sum_{i=0}^{n} 2\,\lambda^{n-i} e(i)x(i-k) = 0 \qquad k = 0,1,\ldots\ldots,p \tag{4.13}$$

Now by replacing *e(n)* and rearranging the eq. (4.14)

$$\sum_{l=0}^{p} w_n(l)\left[\sum_{i=o}^{n} \lambda^{n-i}\, x(i-l)x(i-k)\right] = \sum_{i=o}^{n} \lambda^{n-i}\, d(i)x(i-k) \qquad k = 0,1,\ldots\ldots p \quad (4.14)$$

The above form can be written in terms of matrices as eq. (4.15)

$$R_x(n) = W_n = r_{dx}(n) \quad (4.15)$$

Where $R_x(n)$ is the weighted sample covariance matrix.

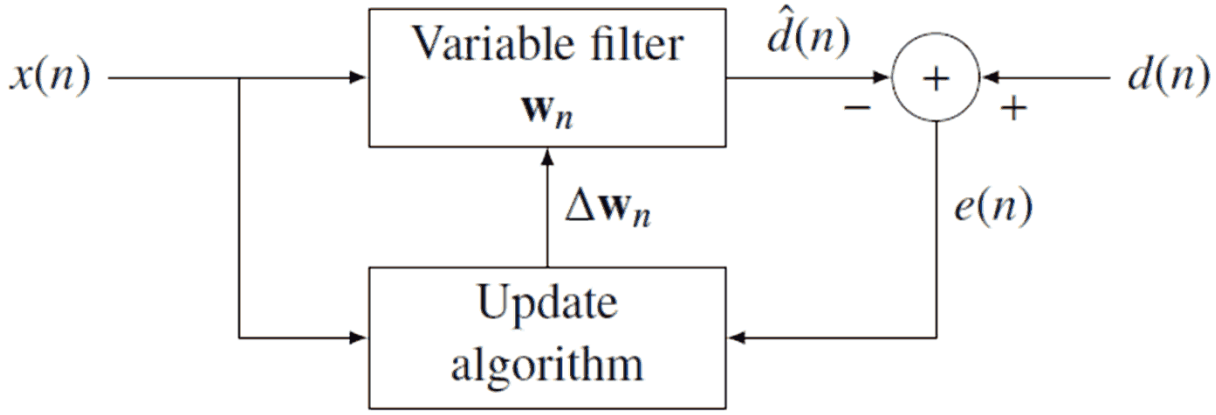

Figure 4.9: Negative feedback diagram

The RLS algorithm for a p-th order RLS filter can be summarized as following.

p = filter order

λ = forgetting factor

δ = value to initialize P(0)

W(n) = 0,

$x(k) = 0, k = -p, \ldots\ldots, -1,$

$d(k) = 0, k = -p, \ldots\ldots, -1,$

$P(0) = \delta I$ where I is the identity matrix of rank p+1

For n= 1, 2, ...

$$x(n) = \begin{bmatrix} x(n) \\ x(n-1) \\ \vdots \\ x(n-p) \end{bmatrix}$$

$$a(n) = d(n) - X^T(n)W(n-1) \tag{4.16}$$

$$g(n) = P(n-1)X(n)\{\lambda + X^T(n)P(n-1)X(n)\}^{-1} \tag{4.17}$$

$$P(n) = \lambda^{-1}P(n-1) - g(n)x^T(n)\lambda^{-1}P(n-1) \tag{4.18}$$

$$W(n) = W(n-1) + a(n)g(n) \tag{4.19}$$

4.10 LEAST MEAN SQUARE

Least mean square is a type of equalizer used to find the filter coefficients producing the least mean square errors which are the errors between the desired and actual signal. It is basically used to calculate the mean square errors between the desired signal and the actual signal output. To understand the LMS we can consider Figure 4.10.

The least square solution for an input matrix X and output vector y is eq. (4.20)

$$\hat{\beta} = (X^T X)^{-1} X^T y \tag{4.20}$$

Most linear adaptive filter problems can be solved using the Figure 4.10.

Where $h(n)$ is to be identified and the adaptive filter will attempt to adapt $\hat{h}(n)$ to make it as close as possible to $h(n)$ by using only observable signals $x(n)$, $d(n)$ and $e(n)$.

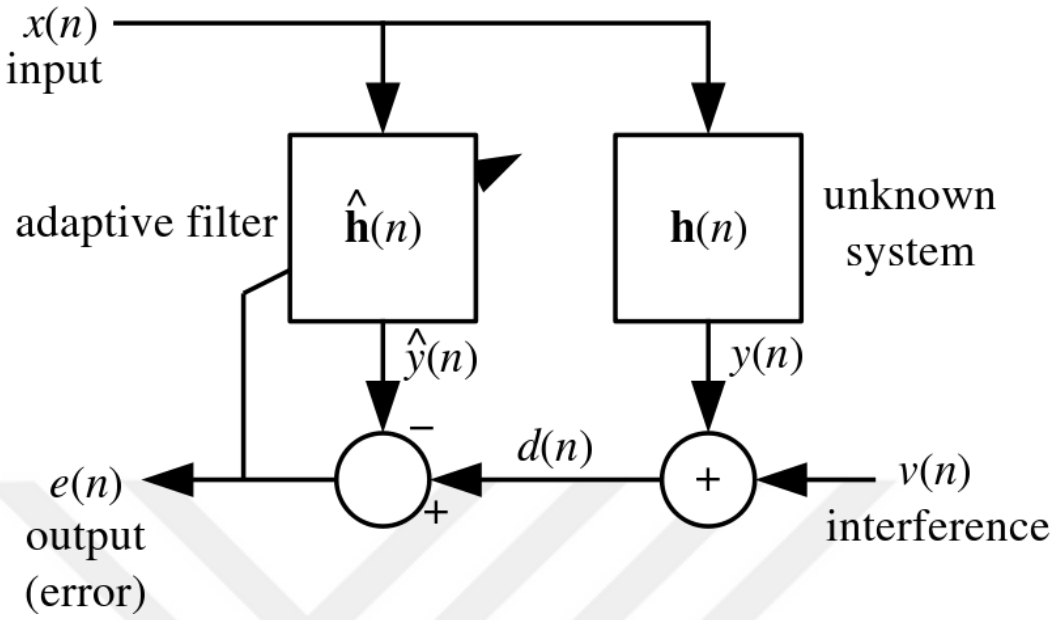

Figure 4.10: Least mean square filter design

Where $y(n)$, $v(n)$ and $h(n)$ is not directly observable.

And

n is the number of input sample

p is the number of filter taps

$\{.\}^H$ is the Hermitian transpose

$$X(n) = [x(n), x(n-1), \ldots\ldots, x(n-p+1)]^T \tag{4.21}$$

$$h(n) = \left[h_o(n), h_1(n), \ldots\ldots, h_{p-1}(n)\right]^T, \quad h(n) \epsilon\, C^p \tag{4.22}$$

$$y(n) = h^H(n).X(n) \tag{4.23}$$

$$d(n) = y(n) + v(n) \tag{4.24}$$

$$e(n) = d(n) - \hat{y}(n) = d(n) - \hat{h}^H(n).X(n) \tag{4.25}$$

$\hat{h}(n)$ represent the estimated filter.

We can summarize the LMS algorithm for p-th order algorithm as follows

p = filter order

μ = step size

$\hat{h}(0) = zeros(p)$

For $n = 0,1,2,\ldots..$

$$X(n) = [x(n), x(n-1), \ldots.., x(n-p+1)]^T \quad (4.21)$$

$$e(n) = d(n) - \hat{h}^H(n)X(n) \quad (4.26)$$

$$\hat{h}(n+1) = \hat{h}(n) + \mu n^*(n)X(n) \quad (4.27)$$

4.11 DECISION FEEDBACK EQUALIZER

Decision feedback is an adaptive filter using feedback of the detected symbols to produce an estimation. It consists of two main parts the forward feedback filter and the feedback filter. The forward filter is a linear filter and the feedback filter is provided with the decision made by the equalized signal. The output of the filter is typically the output subtracted from the output of the linear equalizer. The DFE is used to combat with ISI in the channel.

To properly design the DFE for the best output it is necessary to consider the following steps.

- Input and training signals must be synchronized properly.
- The amplitude of the input and training signals must be the same.
- If the initial coefficients are zeros training mode must be used.

Considering the above rules, a reasonable DFE can be designed to produce the desired output.

4.12 MAXIMUM LIKELIHOOD SEQUENCE ESTIMATION

Maximum likelihood sequence estimation is used to extract required data from a noisy channel. For a perfect detector the aim is not to reconstruct the signal but to extract the signal from the

originally transmitted at the output with minimum or no errors. The MLSE normally tests all possible data sequences and choose the data sequence with the maximum possibility as the output. It normally required a huge computation especially with channels having large delay spread. The block diagram of MLSE is shown in Figure 4.11.

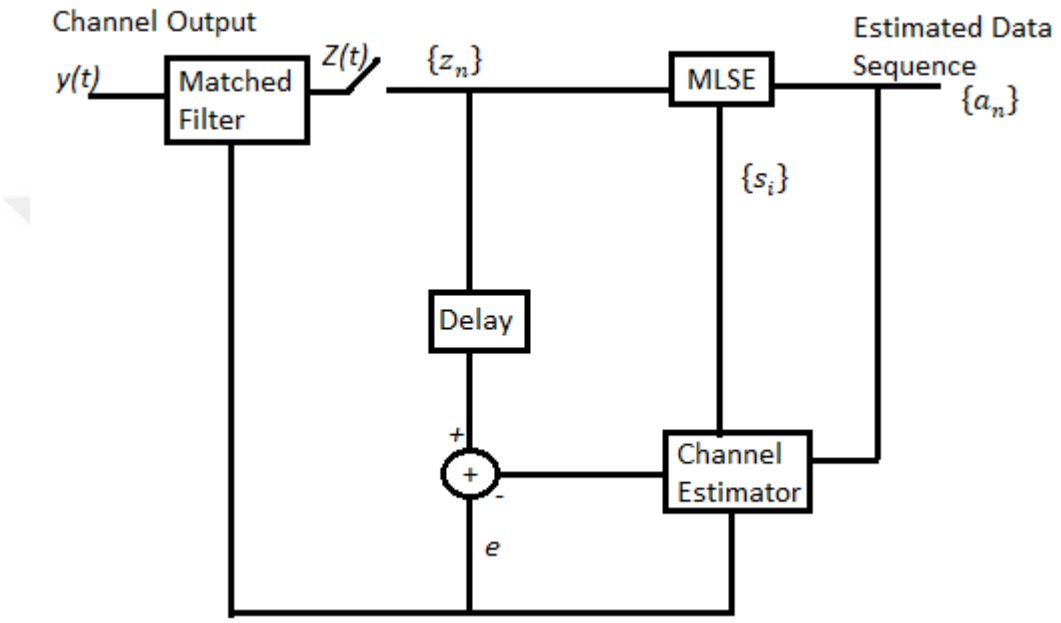

Figure 4.11: Maximum likelihood sequence estimator with adaptive matched filter [4]

4.13 BER PERFORMANCE OF EXPERIMENTAL IN VIVO CHANNEL

In vivo communication is a highly multipath communication that suffers from fading due to the dense structure of the human body, as *in vivo* devices must be placed inside the human body. It is also highly location dependent and a slight change in the position of the device can affect the channel and performance of the system and its link budget. Ultra-wide band frequencies between (3.1 – 10.6 GHz) are used with the central frequency $f_c = 6.75\,GHz$ and bandwidth $BW = 50\,MHz$ for simulations of the experimental data. The complete list of simulation parameters can be found in Table 4.1. Channel response $h(t)$, is extracted by IFFT using eq. (4.28) in MATLAB©. The channel response [66] of the experimental data can be seen in Figure 4.12, which is a 29 taps channel a highly multipath channel with high ISI. The mathematical modeling for the channel is presented in [65].

$$X(n) = \frac{1}{N} * \sum_{K=1}^{N-1} X(K) * e^{i*2*pi*n*\frac{K}{N}} \quad (4.28)$$

Where, *X(K)* represents the frequency domain samples, *X(n)* represent the time domain samples *N* is the size of FFT and *k* is 0,1,2, 3…...N-1.

The signal is modulated using binary phase shift keying (BPSK) modulation with oversampling factor of 4, and can be define as eq. (4.29) [4], root raised cosine (RRC) pulse shaping is used with span = 10 and a roll-off factor of 0.25 using eq. (4.30) [63]. The signal is then convolved with 29 taps *in vivo* channel response, and AWGN is added as noise. At the receiver end, the signal is again demodulated, and BER is calculated for the *in vivo* channel without using any equalization which as expected show the worst channel scenario affected by fading and ISI. The channel is further compared with the ideal AWGN and Rayleigh channel to understand the status of *in vivo* channel and where it lies and which is the closed resembled channel currently available and known in the literature. The BER of BPSK in AWGN is calculated using eq. (4.31). The Rayleigh channel was selected for the comparison as it is used for highly multipath and non-line of side (LOS) fading scenarios, which has a probability density function given in eq. (4.32). All the BER simulations are shown in Figure 4.13.

$$V_{BPSK}(t) = b(t)\sqrt{2P}\cos 2\pi f_c t \quad (4.29)$$

Where 0 < t < T.

And

b(t) = +1 or *-1*, f_c is the carrier frequency, and *T* is the bit duration. The signal has a power $P = \frac{A^2}{2}$, so that$A = \sqrt{2P}$, where A represents the peak value of sinusoidal carrier.

$$H(f) = \begin{cases} \sqrt{T} & \left(0 \le |f| \le \frac{1-\beta}{2T}\right) \\ \sqrt{\frac{T}{2}\left\{1 + \cos\left[\frac{\pi T}{\beta}\left(|f| - \frac{1-\beta}{2T}\right)\right]\right\}} & \left(\frac{1-\beta}{2T} \le |f| \le \frac{1+\beta}{2T}\right) \\ 0 & \left(|f| > \frac{1+\beta}{2T}\right) \end{cases} \quad (4.30)$$

Where *f* is frequency, *T* is the symbol time, and β is the roll-off factor.

$$P_b = \frac{1}{2} erfc\left(\sqrt{\frac{E_b}{N_o}}\right) \tag{4.31}$$

$$p(r) = \begin{cases} \frac{r}{\sigma^2} exp\left(-\frac{r^2}{2\sigma^2}\right), & 0 \le r \le \infty \\ 0, & r < 0 \end{cases} \tag{4.32}$$

Table 4.1: Simulation parameters in MATLAB

Parameters	Values/units
Bandwidth	50MHz
Central Frequency	6.75GHz
S-parameters	S_{21}
Time	μsec
Channel Response	dB
Frequency to Time Domain	IFFT
No of Channel Taps	29
Modulation Scheme	BPSK
Over-Sampling Factor of BPSK	4
Pulse Shaping	RRC
RRC Span	10
RRC Roll Off Factor	0.25
Comparison Channel 1	AWGN
Comparison Channel 2	Rayleigh

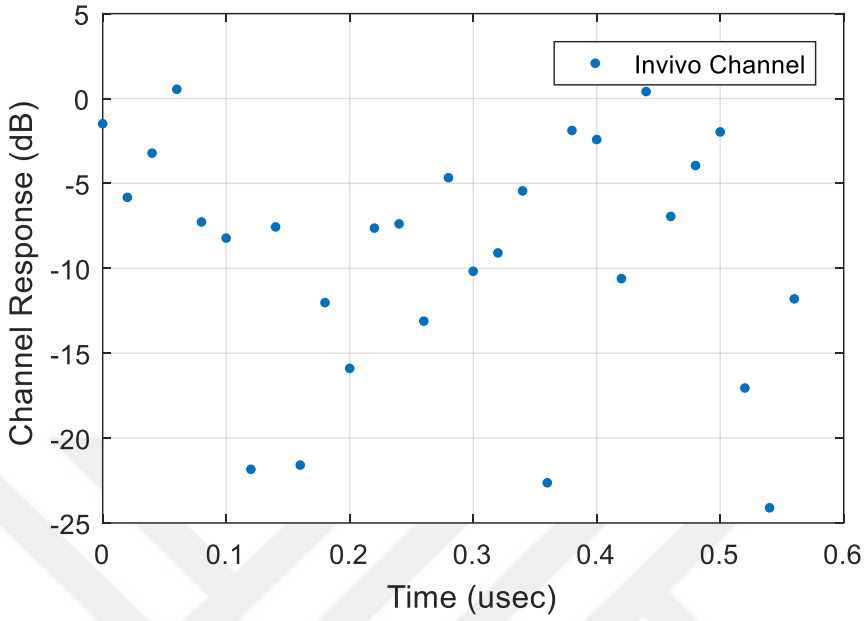

Figure 4.12: Channel response of *in vivo* channel with BW = 50 MHz

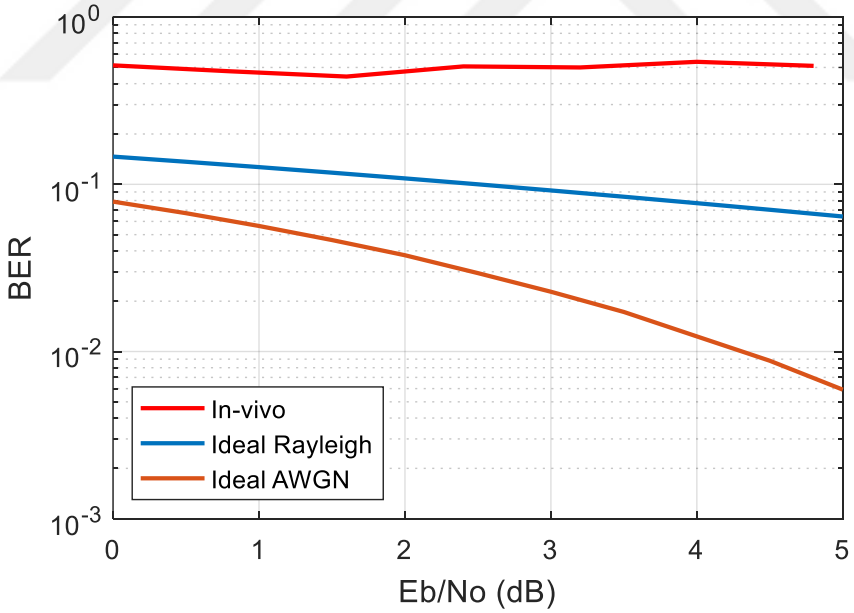

Figure 4.13: BER of *in vivo* channel vs Ideal Rayleigh and Ideal AWGN channels.

A highly multipath channel and high BER is observed in Figure 4.13. In order to improve the BER and obtain our desired performance, equalizer need to be use to improve the BER, this will help improve the BER by compromising the ISI.

4.14 EQUALIZATION OF THE IN VIVO CHANNEL TO IMPROVE BER

Equalization is the process used to render the frequency component of an electronic signal [64]. It helps to get rid of the ISI in the time dispersive and frequency selective channels; those are the channels in which the signal bandwidth is higher than the coherence bandwidth (B_c). ISI introduces distortion in the signal resulting in symbol overlapping which makes it hard for a receiver to distinguish between the desired and undesired symbols causing high BER effecting the performance of the system. An additional reason for an ISI includes multipath scattering environments which are basically non-line of sight signals. Those signals result in the delayed version of a transmitted signal as the signal arrive from a different direction with different power at the receiver and starts interfering with other transmitted symbols. To mitigate the effect of ISI and improve BER, performance equalizers are used to compensate the effect of ISI on a signal.

There are different types of equalization techniques available in the literature to accommodate for different scenarios [54-56]. The most effective ones are the adaptive equalizers distributed as linear and nonlinear equalizers, both of them are used to improve the system performance and to subsequently select the best equalizer for the system. In this research, least mean square equalizer was picked as a linear equalizer combined with recursive least square equalizer and decision feedback equalizer, from the nonlinear equalizers. Some tests were performed using maximum likelihood sequence estimator equalizer (MLSE) equalizer to improve the BER, as in theory MLSE has the best performance, but practically it is the most complicated equalizer [63]. It is observed that for a 29 taps channel MLSE faces memory problems, although with lesser number of taps the MLSE performs better than the LMS and DFE. Considering the number of taps, we only consider LMS and DFE for our tests.

RLS and LMS both are adaptive equalizers, but each of them has its advantages and disadvantages. RLS algorithm converges quickly but the execution takes time, and it is slow as compared to LMS. Where the complexity of the RLS grows roughly with the square of the number of weights which makes it unstable especially in a situation where we need to use higher weights. The RLS algorithm can be summarized with the initialization using eq. (4.33) [4].

$$w(0)=k(0)=x(0)=0,\ R^{-1}(0)=\delta I_{NN} \tag{4.33}$$

Where, I_{NN} is an *NxN* identity Matrix, and δ is a large positive constant. Computing recursively using eq. (4.34-4.38) as follows.

$$w(n) = w(n-1) + k(n)e^*(n) \tag{4.34}$$

$$k(n) = \frac{R^{-1}(n-1)y(n)}{\lambda + y^T(n)R^{-1}(n-1)y(n)} \tag{4.35}$$

$$x(n) = e(n) + \hat{d}(n) \tag{4.36}$$

Where

$$\hat{d}(n) = w^T(n-1)y(n) \tag{4.37}$$

$$R^{-1}(n) = \frac{1}{\lambda}[R^{-1}(n-1) - k(n)y^T(n)R^{-1}(n-1)] \tag{4.38}$$

Where λ represent the weighting coefficient.

The block diagram presenting the structure of RLS equalizers is shown in Figure 4.14.

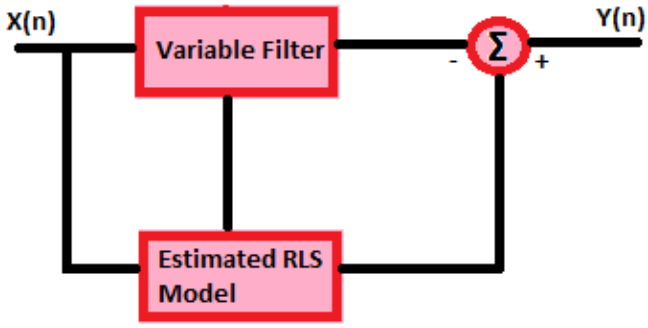

Figure 4.14: RLS block diagram used for equalizing in-vivo signal

While on the other hand, LMS algorithm executes quickly but the convergence process is slow, and the complexity of the LMS increases linearly with respect to weights. LMS can be computed using eq. (4.39-4.41) [4].

$$\hat{d}_k(n) = w^T{}_N(n)y_N(n) \tag{4.39}$$

$$e_k(n) = x_k(n) - \hat{d}_k(n) \tag{4.40}$$

$$w_N(n+1) = w_N(n) - \alpha e^*{}_k(n)y_N(n) \tag{4.41}$$

Where *n* represents a sequence of iterations, *N* number of delay stages and α is step size.

The block diagram presenting the structure of LMS is shown in Figure 4.15.

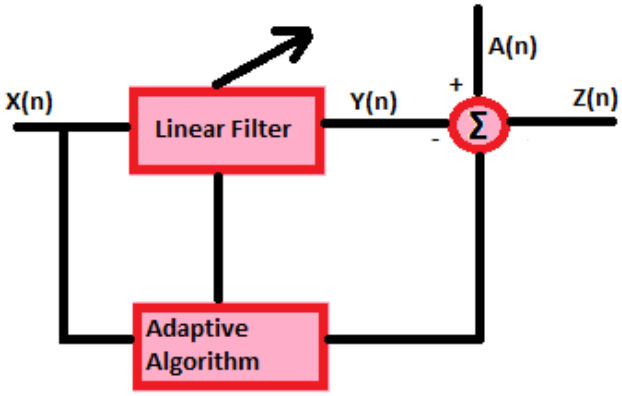

Figure 4.15: LMS block diagram used for equalizing in-vivo signal.

The goal of the least mean square equalizer is to minimize the mean square error (MSE) presented in the output of the equalizer. The prediction of error is highly dependent on the tap gain such that the MSE of the equalizer output is the function of weight. The recursive least square on the other hand requires the calculation of tap gain vector so that the cumulative square error can be minimized.

While for the nonlinear equalizer, decision feedback equalizer is used which has $N_1 + N_2 + 1$ taps in the feedforward filter and N_3 taps in the feedback producing an output eq. (4.42). The main idea of DFE is to estimate and subtract the symbols which will introduce ISI on future symbols [4].

$$\hat{d}_k = \sum_{n=-N_1}^{N_2} c^*{}_n y_{k-n} + \sum_{i=1}^{N_3} F_i \, d_{k-i} \tag{4.42}$$

Where $c^*{}_n$ and y_n are tap gain and the input $f^*{}_i$ tap gain input for feedback. $d_i (i < k)$ is the previous decision made on the detected signal. The minimum mean square error (MSE) a DFE can be achieved is eq. (4.43)

$$E[|e(n)|^2]_{min} = exp\left\{\frac{T}{2\pi}\int_{\frac{-\pi}{T}}^{\frac{\pi}{T}} ln\left[\frac{N_o}{|F(e^{jwT})|^2 + N_o}\right] d\omega\right\} \tag{4.43}$$

The recursive least square and least mean square algorithms are used together by exploiting their properties of quick convergence (RLS) and fast execution (LMS), which help the simulation to execute quickly and present better results.

4.15 SIMULATIONS AND RESULTS DISCUSSION

The general requirement for implementation of adaptive equalizers consists of a number of taps, step size, signal constellation (BPSK in our case) and an initial set of weights for equalizers taps after which the block adaptively update the weights continuously throughout the simulation. To equalize the signal, an equalization object needs to be created which consists of the desired equalizer, and the algorithms needed to be used, it can then be applied to the desired channel that needs to be equalized.

We mainly used two adaptive equalizers in our simulations to test their performance on *in vivo* channel to improve the BER. First, the channel frequency response is plotted by normalizing the magnitude and the frequency of the signal as shown in Figure 4.17. A frequency selective channel is observed; this issue is previously discussed by Demir *et al.* [23] a mean RMS delay spread of *2.76 ns* is observed using eq. (4.45) and the coherence bandwidth ($B_c = 7.25\ MHz$) is calculated using eq. (4.47).

The mean excess delay can be calculated using eq. (4.44).

$$\bar{\tau}=\frac{\sum_k p(\tau_k)\tau_k}{\sum_k p(\tau_k)} \tag{4.44}$$

And, The RMS delay spread is defined as eq. (4.45)

$$\sigma_\tau = \sqrt{\overline{\tau^2} - (\bar{\tau})^2} \tag{4.45}$$

Where

$$\overline{\tau^2} = \frac{\sum_k p(\tau_k)\tau_k{}^2}{\sum_k p(\tau_k)} \tag{4.46}$$

$$B_c \approx \frac{1}{50\sigma_\tau} \tag{4.47}$$

This is not critical for a narrow band (NB) communication but it can cause issues while working with ultra-wideband. As in our case, we are working on the $BW = 50\ \ MHz$ which is much higher than the calculated B_c and makes the signal frequency selective.

The block diagram presented in Figure 4.16 is showing the equalizers structure used to improve the BER performance of the *in vivo* radio channel. The basic limitations with the linear equalizers is their poor performance on the channel having spectral nulls. Decision feedback equalizer is a non-linear equalizer and has the advantage to subtract the distortion on a current pulse that is caused by the previous pulses. In the block diagram of DFE, the forward filter and the feedback filter can be both linear filters and are working as a linear filter while working separately but the non-linearity of decision feedback is because of the non-linear properties of the detector. The main idea of DFE is if the values of the symbols previously detected are known it can be used to cancel the ISI right at the output of the feedforward filter. In order to minimize the mean square error, the weights of the feedforward and feedback filters can be adjusted simultaneously to produce better results.

So if we send a single bit from a transmitter and pass it through the channel, the channels act like a low pass filter and it smears the transmitted bit and introduce inter-symbol interference. The DFE is used to subtract that smearing, which comes from the previous bit. So it slices the bit and delayed it by one-unit interval multiply it by a constant that represent the amount of smearing and finally subtract that amount from the next bit, which helps return a voltage closer to the true value.

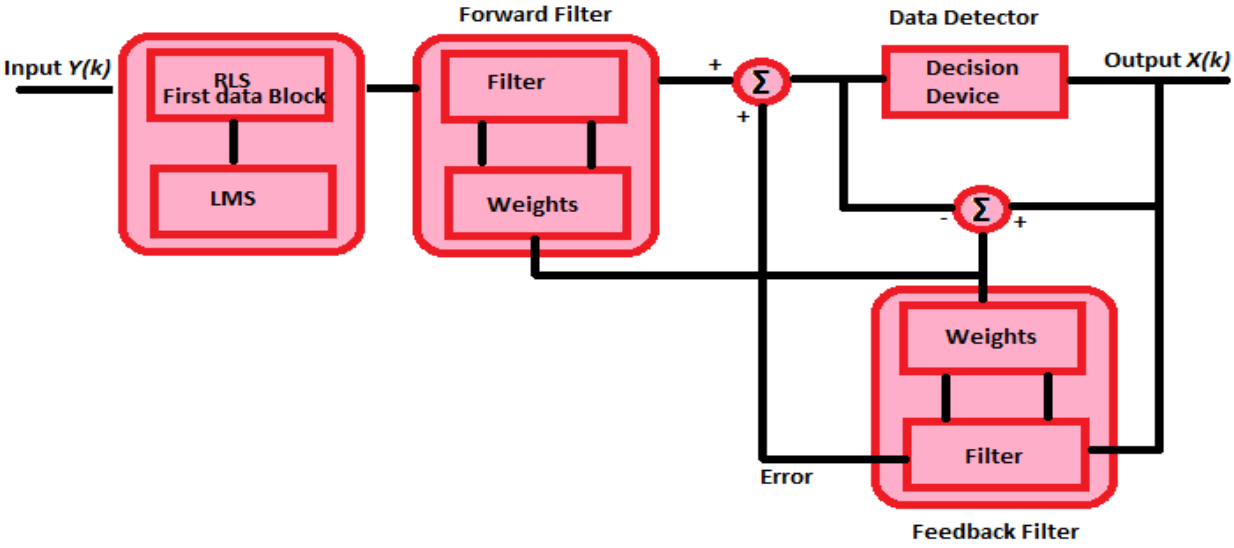

Figure 4.16: Block diagram of equalizers used to improve the BER performance of experimental in vivo radio channel.

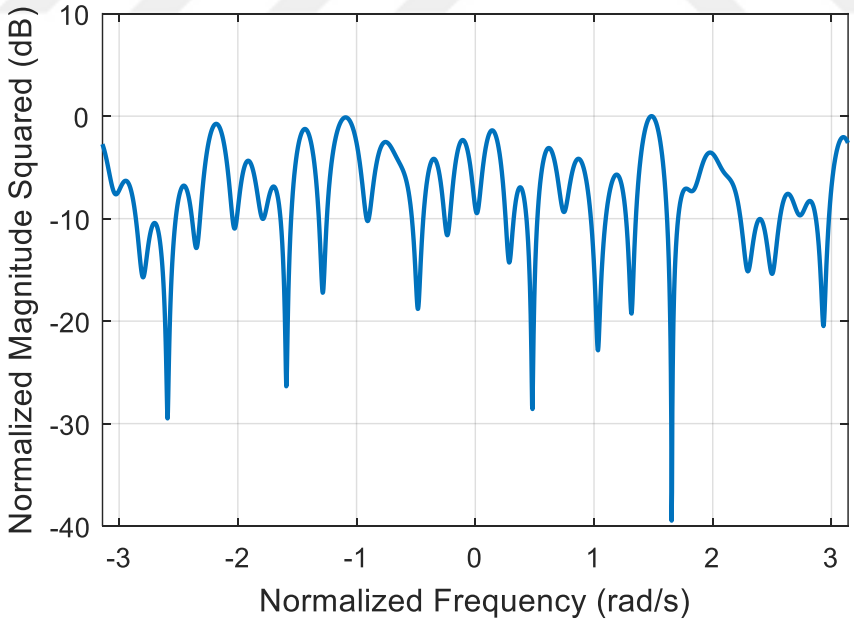

Figure 4.17: Un-equalized *in vivo* channel frequency response. for in –vivo channel.

Considering pros and cons of both the RLS and LMS discussed in the previous section we decided to use the properties of both of these algorithms to achieve quick and better results. RLS converges faster than LMS and LMS can be executed quickly. The parameter values for LMS

and DFE are set by using 55 taps linear equalizer and 29 taps feedforward and 29 taps feedback weights for DFE. The detailed list of the parameter are shown in Table 4.2. RLS is used only for the first data block at each Eb/No which helped us rapidly converge the taps and LMS algorithm is used for the remaining data blocks in order to ensure rapid execution speed.

A linear equalizer object is constructed and implemented in the simulations for both LMS and DFE. First, the simulation for the linear equalizer is executed and the equalizer signal spectrum of a linearly equalized signal can be seen in Figure 4.18. It is observed that as the Eb/No increases the spectrum has a deeper null, which point us to the fact that a linear equalizer must use more taps to get better performance. After that, the DFE equalizer has been executed and the signal spectrum for DFE is plotted as shown in Figure 4.19. It is observed that at low BER DFE suffers from error bursts but later it shows dynamically improved results compare to LMS. DFE performs much more effectively on the *in vivo* channel as compared to the LMS by mitigating the channel null better than LMS. The DFE errors bursts were higher compared to LMS that is because of its feedback detection of bits instead of the correct bits.

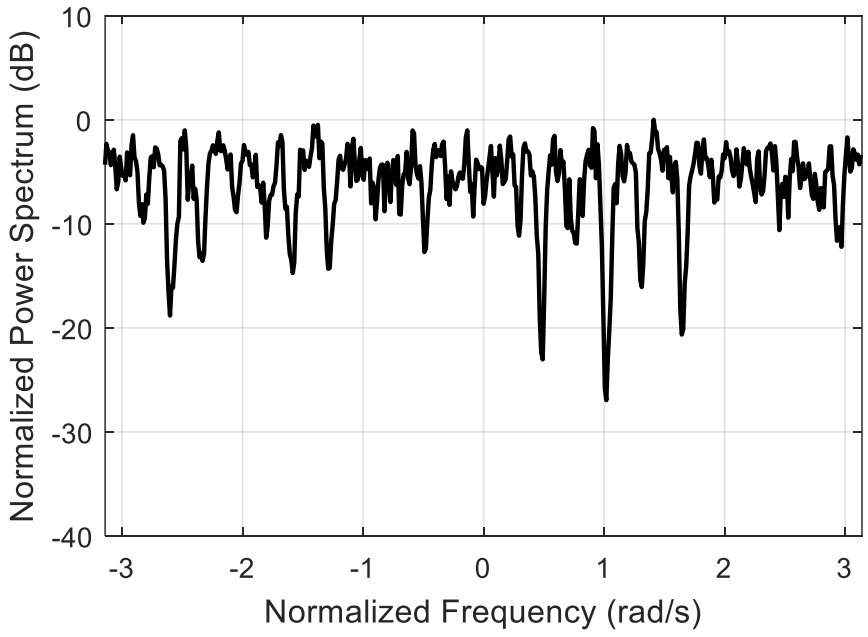

Figure 4.18: Linearly equalized signal power spectrum for in –vivo channel.

Two types of power spectrums are extracted using power spectral density (PSD) functions. Power spectral density or power spectrum are used to characterize random processes in

frequency domain. The power spectrum $S(\omega)$ is actually the Discrete Time Fourier Transform (DTFT) of the correlation sequence $r[k]$ for the process. The power spectral density can be defined as eq. (4.48).

$$S(\omega) = \sum_{k=-\infty}^{\infty} r[k]e^{-jk\omega} \tag{4.48}$$

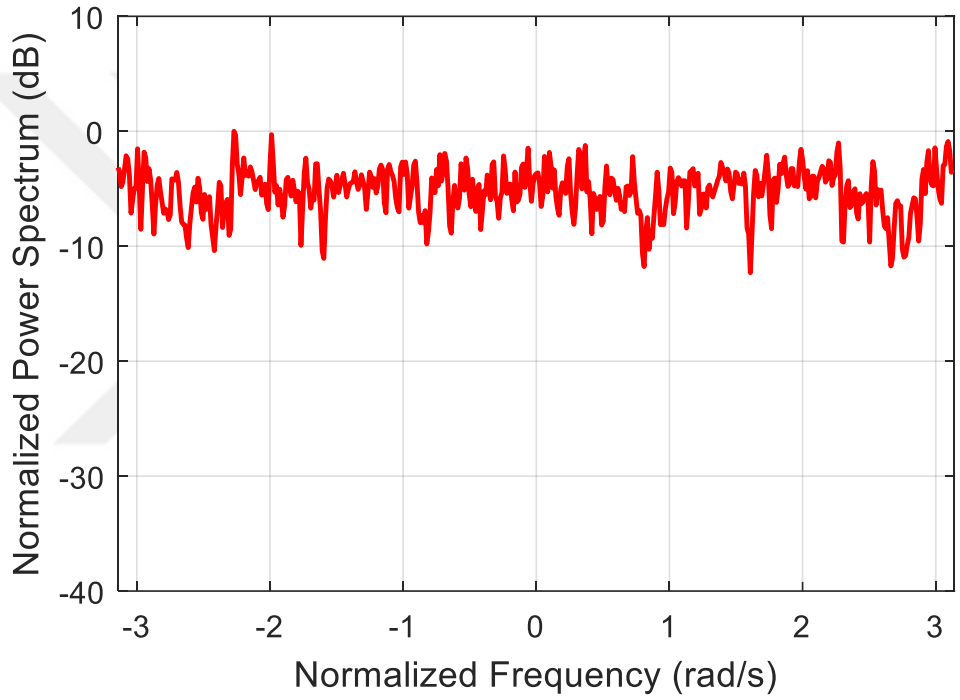

Figure 4.19: DFE signal power spectrum for in –vivo channel.

Or equivalently

$$r[k] = \frac{1}{2\pi}\int_{-\pi}^{\pi} S(\omega)e^{jk\omega}d\omega \tag{4.49}$$

In terms of an interpretation, if the power spectrum is integrated between ω_a and ω_b and called that P_{ab} and normalized it by 2π, the quantity will represent the expected contribution to total power or variance due to components of the random process between theses points ω_a and ω_b and can be represented as eq. (4.50)

$$P_{ab} = \frac{1}{2\pi} \int_{\omega_a}^{\omega_b} S(\omega)\, d\omega \tag{4.50}$$

Hence, by finding the area under $S(\omega)$ between ω_a and ω_b that's the power of this portion of the spectrum is expected to contribute the random process, which tells us how the contribution of the power are distributed in frequency.

The power spectrum is actually the density, hence the units in terms of radian frequency will be represented as $S(f) = power/radian$ and the frequency that measured the units of hertz will be presented as $S(f) = power/hertz$.

The total power can be represented as eq. (4.51)

$$r[0] = \frac{1}{2\pi} \int_{-\pi}^{\pi} S(\omega)\, d\omega = E\{x^2[n]\} \tag{4.51}$$

Where the power cannot be zero.

$$S(\omega) \geq 0 \quad non\ negative$$

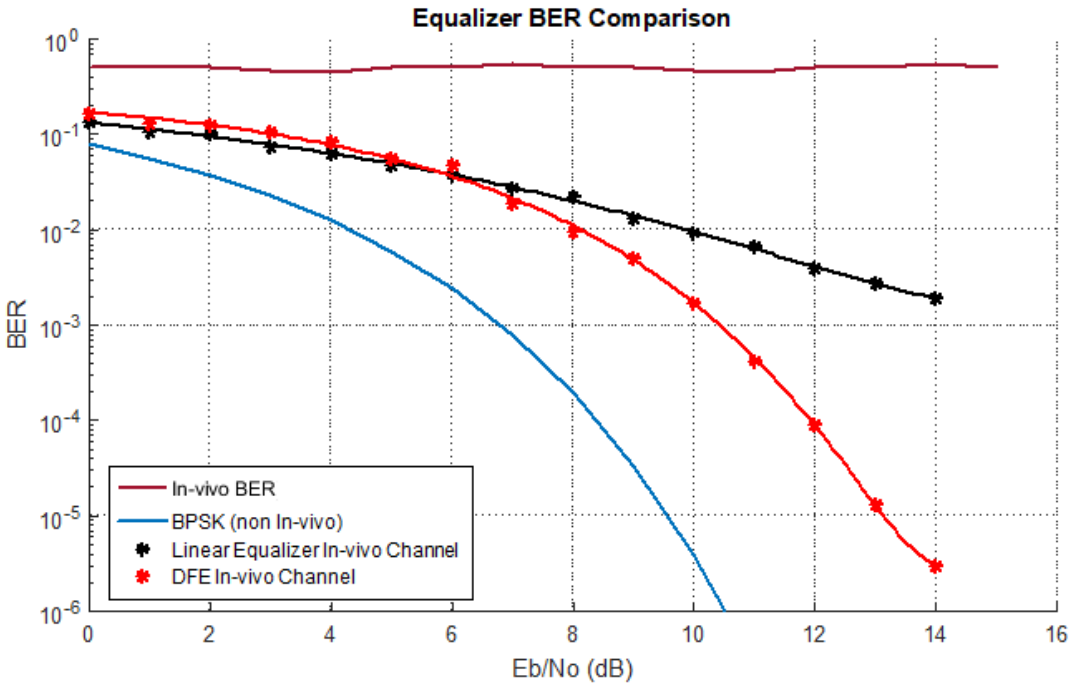

Figure 4.20: Equalizers BER performance comparison along with ideal BPSK

Hence by comparing the power spectrums, both linearly equalized and decision feedback equalizer power spectrum, it can be seen that the maximum fluctuation observed in un equalized frequency response is between 0 dB to -40 dB. Where the linear equalization reduces it between 0 dB to -30 dB. Although DFE outperformed the LMS and presents the best results by keeping the power spectrum between 0 dB to -10 dB. These results show that a non-linear decision feedback equalizer offers better performance than the recursive least square and least mean square combined. As the power spectrum was improved by 25% using least mean square and 75% using decision feedback equalizer considering the highest fluctuated peaks. Although the analysis is based on the maximum peaks but the overall fluctuation of the power spectrum using Figure 4.18 for linearly equalized least mean square is between 0 dB to -10 dB and 0 to -20 dB in that case part of the spectrum is recovered between 50% to 75%. While in the case of decision feedback, it remains the same throughout the simulation as shown in Figure 4.19, which shows better and stable performance of decision feedback compared to least mean square.

Table 4.2: Simulation parameters for equalization in MATLAB

Parameters	Values/units
Sampling Frequency F*s*	1
Modulation	BPSK
Symbol Rate *Rs*	1
Sample Per Symbol	*Fs/Rs*
No of Channel Taps	29
Eb/No	0-14 (dB)
No of Weights	55
RLS Algorithm	1 Data Block
LMS Step Size	0.00001
DFE Feedforward Weights	29
DFE Feedback Weights	29

Finally, the BER results are shown for both LMS and DFE equalizers in Figure 4.20 along with the ideal BPSK as a comparison. It can be clearly observed that DFE easily outperformed the BER performance compare to LMS. It can be concluded that non-linear equalizers performed better for *in vivo* channels as compare to linear equalizers. Although with low Eb/No initially the LMS performance was slightly better than DFE but at Eb/No = 6 dB and so on DFE shows a much better BER results compared to LMS [67].

The detailed analysis with exact quantitative values for the bit error rate performance comparison between least mean square equalizer and decision feedback equalizer are presented in Table 4.3. It can be clearly seen from the values that the ideal binary phase shift keying has the best performance in its ideal state. Initially the least mean square equalizer show better performance as compared to the decision feedback algorithm. The linear mean square was incorporated with recursive least square algorithm in order to converge the system quickly and the LMS further take the operation to execute it rapidly. The results of LMS was slightly better until Eb/No = 6, afterwards the decision feedback equalizer present significant performance compared to the least mean square and dramatically improve the bit error rate.

Table 4.3: BER results

Eb/No	Ideal BPSK	Linear Equalizer	Decision Feedback Equalizer
0	0.07865	0.1317	0.1684
2	0.03751	0.09441	0.1247
4	0.0125	0.06248	0.08358
6	0.00238	0.03648	0.0472
8	0.00019	0.02187	0.00956
10	$3.872e^{-6}$	0.00948	0.00168
12	N/A	0.00388	$8.721e^{-05}$
14	N/A	0.001903	$3.013e^{-06}$

5 CONCLUSION

This research present experimental channel response for *in vivo* communication. The simulations in this research will help the researchers understand the real *in vivo* channel response and its effects on the WBAN's. It is concluded that *in vivo* is a multipath channel and can be highly changeable with the change in position of the antenna even if it is at a small distance. The reported analysis highlights the challenges for modelling those types of channels and open a way for further studies in such environment.

A novel mathematical model for UWB in-vivo radio channel. Blind testing is performed on the proposed model. The statistics of the error for the blind test using proposed model is RMSE 7.76. This validates the accuracy of the proposed while applying on different channel response. The presented analysis highlights a novel method to obligate the communication challenges in such environment and will help system designer to develop an accurate link budget calculation without going for costly experiments and time-consuming simulation and will open a way for further studies in this undesired environment.

A detailed analysis and improvement of *in* vivo radio channel BER performance with and without different equalizers is also part of this research, which shows the similarity between the *in* vivo channels that do not use any equalizers and the Rayleigh channel. Both channels suffer from severe fading due to the non-line of sight situation. Furthermore, different equalizers were used to test their performance for improving BER performance of an in *vivo channel and* compromise the effect of ISI caused by using the UWB technology. It is clear that the *in* vivo channel is a frequency selective channel that will suffer from ISI with ultra-wideband communication. Therefore, equalizers must be used to compensate for the effects of the ISI. This provides a preliminary insight of *in vivo* communication. The presented analysis offers novel results and findings to obligate the communication and can help guide future research that may acquire more time, resources and challenges in such environment. This study can be used as a stepping stone for comprehensive and thorough studies in this undesired fading environment.

REFERENCES

[1] F. Demir *et al*., "In Vivo Communications: Steps Toward the Next Generation of Implantable Devices," in *IEEE Vehicular Technology Magazine,* vol. 11, no. 2, pp. 32-42, June 2016.

[2] W. Great batch and C. F. Holmes, "History of implantable devices," in *IEEE Engineering in Medicine and Biology Magazine*, vol. 10, no. 3, pp. 38-41, Sept. 1991.

[3] Q. H. Abbasi *et al*., "Nano-Communication for Biomedical Applications: A Review on the State-of-the-Art From Physical Layers to Novel Networking Concepts," in *IEEE Access*, vol. 4, pp. 3920-3935, 2016.

[4] T. S. Rappaport, Wireless Communications: Principles and Practice, vol. 2, 1996.

[5] W. Viriyasitavat, M. Boban, H. M. Tsai and A. Vasilakos, "Vehicular Communications: Survey and Challenges of Channel and Propagation Models," in *IEEE Vehicular Technology Magazine*, vol. 10, no. 2, pp. 55-66, June 2015.

[6] Q. H. Abbasi, A. Sani, A. Alomainy and Y. Hao, "On-Body Radio Channel Characterization and System-Level Modeling for Multiband OFDM Ultra-Wideband Body-Centric Wireless Network," in *IEEE Transactions on Microwave Theory and Techniques*, vol. 58, no. 12, pp. 3485-3492, Dec. 2010.

[7] J. M. Molina-Garcia-Pardo, M. Lienard, A. Nasr and P. Degauque, "Wideband analysis of large scale and small scale fading in tunnels," *2008 8th International Conference on ITS Telecommunications*, Phuket, 2008, pp. 270-273.

[8] Daeyoung Kim, M. A. Ingram and W. W. Smith, "Measurements of small-scale fading and path loss for long range RF tags," in *IEEE Transactions on Antennas and Propagation*, vol. 51, no. 8, pp. 1740-1749, Aug. 2003.

[9] T. K. Sarkar, Zhong Ji, Kyungjung Kim, A. Medouri and M. Salazar-Palma, "A survey of various propagation models for mobile communication," in *IEEE Antennas and Propagation Magazine*, vol. 45, no. 3, pp. 51-82, June 2003.

[10] Qammer H. Abbasi, Masood Ur Rehman, Khalid Qaraqe and Akram Alomainy,"Advances in Body-Centric Wireless Communications: Applications and State-ofthe-art", The Institution of Engineering and Technolog (IET) Publication, July, 2016, ISBN: 978-1-84919-989-6 (print), ISBN 978-1-84919-990-2

[11] S. Movassaghi, M. Abolhasan, J. Lipman, D. Smith and A. Jamalipour, "Wireless Body Area Networks: A Survey," in *IEEE Communications Surveys & Tutorials*, vol. 16, no. 3, pp. 1658-1686, Third Quarter 2014.

[12] B. Latrc, B. Braem, J. Moerman, C. Blondia, P. Demeester, "A survey on wireless body area networks", *Wireless Network,* vol. 17, pp. 1-18, Jan. 2009.

[13] M. Hanson, H. Powell, A. Barth, K. Ringgenberg, B. Calhoun, J. Aylor, J. Lach, "Body area sensor networks: Challenges and opportunities", *Computer*, vol. 42, pp. 58-65, Jan. 2009.

[14] R. Li, D. T. H. Lai and W. Lee, "A Survey on Biofeedback and Actuation in Wireless Body Area Networks (WBAN)," in *IEEE Reviews in Biomedical Engineering*, vol. PP, no. 99, pp. 1-1, Aug. 2017.

[15] Otto, A. Milenkovic, C. Sanders, E. Jovanoy, "System architecture of a wireless body area sensor network for ubiquitous health monitoring", *J. Mob. Multimed,* vol. 1, pp. 307-326, Jan. 2005.

[16] A. Milenkovic, C. Otto, E. Jovanov, "Wireless sensor networks for personal health monitoring: Issues and an implementation", *Computer Communications*, vol. 29, pp. 2521-2533, 2006.

[17] H. J. Yoo, "Wireless body area network and its healthcare applications," *2013 Asia-Pacific Microwave Conference Proceedings (APMC)*, Seoul, 2013, pp. 89-91.

[18] R. Chávez-Santiago, A. Khaleghi, I. Balasingham and T. A. Ramstad, "Architecture of an ultra-wideband wireless body area network for medical applications," *2009 2nd International Symposium on Applied Sciences in Biomedical and Communication Technologies*, Bratislava, 2009, pp. 1-6.

[19] S. Ullah, B. Shen, S: M. R. Islam, P. Khan, S. Saleem, K. S. Kwak, "A study of medium access control protocols for wireless body area networks", 2010.

[20] S. L. Cotton and W. G. Scanlon, "A Statistical Analysis of Indoor Multipath Fading for a Narrowband Wireless Body Area Network," *2006 IEEE 17th International Symposium on Personal, Indoor and Mobile Radio Communications*, Helsinki, 2006, pp. 1-5.

[21] H. Y. Lin, M. Takahashi, K. Saito, K. Ito, "Characteristics of electric field and radiation pattern on different locations of the human body for in-body wireless communication", IEEE Trans. Antennas propag. Vol. 61, no. 10, pp. 5350-5354, Oct. 2013.

[22] C. Anzai et al., "Experimental evaluation of implant UWB-IR transmission with living animals for body area networks", *IEEE Trans. Microw. Theory Tech.*, vol. 62, no. 1, pp. 183-192, Jan. 2014.

[23] Demir, A. F., Abbasi, Q. H., Ankarali, Z. E., Alomainy, A., Qaraqe, K., Serpedin, E. and Arslan, H., "Anatomical Region-Specific In Vivo Wireless Communication Channel Characterization," in *IEEE Journal of Biomedical and Health Informatics*, vol. 21, no. 5, pp. 1254-1262, Sept. 2017.

[24] Q. H. Abbasi, A. Sani, A. Alomainy and Y. Hao, "On-Body Radio Channel Characterization and System-Level Modeling for Multiband OFDM Ultra-Wideband Body-Centric Wireless Network," in *IEEE Transactions on Microwave Theory and Techniques*, vol. 58, no. 12, pp. 3485-3492, Dec. 2010.

[25] A. F. Demir, Z. E. Ankarali, Y. Liu, Q. H. Abbasi, K. Qaraqe, E. Serpedin, H. Arslan, and R. D. Gitlin, "In Vivo Wireless Channel Modeling", Book Chapter, *Advances in Body-Centric Wireless Communication: Applications and state-of-the-art*, The Institution of Engineering and Technology, 2016, pp. 187-211, ISBN: 978-1-84919-989-6.

[26] Huan Wang, "Wireless body area networks path loss characterization analysis," *2010 2nd International Conference on Computer Engineering and Technology*, Chengdu, 2010, pp. V2-163-V2-164.

[27] M. R. Basar et al., "The use of a human body model to determine the variation of path losses in the human body channel in wireless capsule endoscopy", *Progress Electromagn. Res.*, vol. 133, pp. 495-513, 2013.

[28] D. Smith, L. Hanlen, "Wireless body area networks: Towards a wearable intranet", *ISCIT Tutorial*, Sept. 2012.

[29] S. Ullah, H. Higgin, M. A. Siddiqui, K. S. Kwak, "A study of implanted and wearable body sensor networks", *Porc. 2nd KES Int. Conf. on Agent and multi-agent systems: technologies and aapplications*, pp. 464-473, 2008.

[30] F. Tufail and M. H. Islam, "Wearable Wireless Body Area Networks," *2009 International Conference on Information Management and Engineering*, Kuala Lumpur, 2009, pp. 656-660.

[31] Q. H. Abbasi, H. El Sallabi, N. Chopra, K. Yang, K. A. Qaraqe and A. Alomainy, "Terahertz Channel Characterization Inside the Human Skin for Nano-Scale Body-Centric Networks," in *IEEE Transactions on Terahertz Science and Technology*, vol. 6, no. 3, pp. 427-434, May 2016.

[32] R. Zhang, K. Yang, Q. H. Abbasi, K. A. Qaraqe and A. Alomainy, "Analytical Characterisation of the Terahertz In-Vivo Nano-Network in the Presence of Interference Based on TS-OOK Communication Scheme," in *IEEE Access*, vol. 5, pp. 10172-10181, 2017.

[33] W. Greatbatch and C. F. Holmes, "History of implantable devices," in *IEEE Engineering in Medicine and Biology Magazine*, vol. 10, no. 3, pp. 38-41, Sept. 1991.

[34] P. Anacleto, P. M. Mendes, E. Gultepe and D. H. Gracias, "Micro antennas for implantable medical devices," *2013 IEEE 3rd Portuguese Meeting in Bioengineering (ENBENG)*, Braga, 2013, pp. 1-4.

[35] T. Xu, J. B. Wendt and M. Potkonjak, "Matched Digital PUFs for Low Power Security in Implantable Medical Devices," *2014 IEEE International Conference on Healthcare Informatics*, Verona, 2014, pp. 33-38.

[36] Y. X. Guo, D. Zhu and R. Jegadeesan, "Inductive wireless power transmission for implantable devices," *2011 International Workshop on Antenna Technology (iWAT)*, Hong Kong, 2011, pp. 445-448.

[37] J. I. Al-Nabulsi, H. A. Al-Doori and N. T. Salawy, "Human motion to recharge implantable devices," *2017 10th Jordanian International Electrical and Electronics Engineering Conference (JIEEEC)*, Amman, 2017, pp. 1-5.

[38] D. Halperin, T. S. Heydt-Benjamin, K. Fu, T. Kohno and W. H. Maisel, "Security and Privacy for Implantable Medical Devices," in *IEEE Pervasive Computing*, vol. 7, no. 1, pp. 30-39, Jan.-March 2008.

[39] R. Yan, T. Xu and M. Potkonjak, "Semantic attacks on wireless medical devices," *IEEE SENSORS 2014 Proceedings*, Valencia, 2014, pp. 482-485.

[40] C. Garcia-Pardo *et al.*, "Experimental ultra wideband path loss models for implant communications," *2016 IEEE 27th Annual International Symposium on Personal, Indoor, and Mobile Radio Communications (PIMRC)*, Valencia, 2016, pp. 1-6.

[41] K. Sayrafian-Pour, W.-B. Yang, J. Hagedorn, J. Terrill, K. Yekeh Yazdandoost, K. Hamaguchi, "Channel Models for Medical Implant Communication", *International Journal of Wireless Information Networks*, vol. 17, no. 3, pp. 105-112, 2010.

[42] E. Chow *et al*., "Commercial development of RF medical implantable devices," *2013 IEEE MTT-S International Microwave Workshop Series on RF and Wireless Technologies for Biomedical and Healthcare Applications (IMWS-BIO)*, Singapore, 2013, pp. 1-3.

[43] T. P. Ketterl, G. E. Arrobo, A. Sahin, T. J. Tillman, H. Arslan and R. D. Gitlin, "In vivo wireless communication channels," *WAMICON 2012 IEEE Wireless & Microwave Technology Conference*, Cocoa Beach, FL, 2012, pp. 1-3.

[44] K. Hassan, J. G. Andrews and W. Frey, "In-vivo communication using blood vessels as the transport channel," *2009 Conference Record of the Forty-Third Asilomar Conference on Signals, Systems and Computers*, Pacific Grove, CA, 2009, pp. 55-59.

[45] Naveed A. Abbasi, Dilan Lafci and Ozgur B. Akan, "Controlled Information Transfer Through an *In vivo* Nervous System," Feb. 2018 Nature, Scientific Reports 8, Article No. 2298, doi: 10.1038/s41598-018-20725-2.

[46] T. P. Ketterl, G. E. Arrobo and R. D. Gitlin, "SAR and BER evaluation using a simulation test bench for in vivo communication at 2.4 GHz," *WAMICON 2013*, Orlando, FL, 2013, pp. 1-4.

[47] C. He, Y. Liu, G. E. Arrobo, T. P. Ketterl and R. D. Gitlin, "In vivo wireless communications and networking," *2015 Information Theory and Applications Workshop (ITA)*, San Diego, CA, 2015, pp. 163-172.

[48] M. R. Mahfouz and M. J. Kuhn, "UWB channel measurements and modeling for positioning and communications systems in the operating room," *2011 IEEE Topical Conference on Biomedical Wireless Technologies, Networks, and Sensing Systems*, Phoenix, AZ, 2011, pp. 47-50.

[49] Q. H. Abbasi, M. Qaraqe, M. U. Rehman and E. Serpedin, "Ultra wideband in vivo radio channel characterisation and system modeling," *2014 IEEE MTT-S International Microwave Workshop Series on RF and Wireless Technologies for Biomedical and Healthcare Applications (IMWS-Bio2014)*, London, 2014, pp. 1-3.

[50] M. Rupp and J. A. Garcia-Naya, "Equalizers in mobile communications: Tutorial 38," in *IEEE Instrumentation & Measurement Magazine*, vol. 15, no. 3, pp. 32-42, June 2012.

[51] M. Martinez-Ramon, A. Artes-Rodriguez, A. Navia-Vazquez and A. R. Figueiras-Vidal, "Adaptively combined LMS and logistic equalizers," in *IEEE Signal Processing Letters*, vol. 11, no. 10, pp. 777-779, Oct. 2004.

[52] G. Ysebaert, K. Vanbleu, G. Cuypers, M. Moonen and T. Pollet, "Combined RLS-LMS initialization for per tone equalizers in DMT-receivers," in *IEEE Transactions on Signal Processing*, vol. 51, no. 7, pp. 1916-1927, July 2003.

[53] A.Razavi, "The Decision-Feedback Equalizer [A Circuit for All Seasons]," in *IEEE Solid-State Circuits Magazine*, vol. 9, no. 4, pp. 13-132, Fall 2017.

[54] A.H. Mehana and A. Nosratinia, "New results in the analysis of decision-feedback equalizers," *2013 Asilomar Conference on Signals, Systems and Computers*, Pacific Grove, CA, 2013, pp. 2118-2121.

[55] Chih-Hsiu Lin and An-Yeu Wu, "Low cost decision feedback equalizer (DFE) design for Giga-bit systems," *Proceedings. (ICASSP '05). IEEE International Conference on Acoustics, Speech, and Signal Processing, 2005.*, 2005, pp. iii/1001-iii/1004 Vol. 3.

[56] Z. Chen, "Decision Feedback Equalizer (DFE) behavioral macro model for packaging system eye diagram transient simulations," *2011 IEEE 61st Electronic Components and Technology Conference (ECTC)*, Lake Buena Vista, FL, 2011, pp. 209-216.

[57] O. Bayat, B. Shafai and O. N. Ucan, "Reduced state equalization of multilevel turbo coded signals," *Proceedings. (ICASSP '05). IEEE International Conference on Acoustics, Speech, and Signal Processing, 2005.*, 2005, pp. iii/705-iii/708 Vol. 3.

[58] O. Bayat, B. Shafai and O. N. Ucan, An Efficient Channel Equalization on the Transmission of Turbo Coded Signals, *proceedings of CIC Conference*, Las Vegas, Nevada, USA, June 2004.

[59] O. Bayat, "Intersymsol interference cancellation in CDMA 1xEVDO network," International Journal of communication systems, 2014, issue 10, vol. 27, pp. 1553-1560.

[60] A. F. Demir, Q. H. Abbasi, Z. E. Ankarali, M. Qaraqe, E. Serpedin and H. Arslan, "Experimental Characterization of In Vivo Wireless Communication Channels," *2015 IEEE 82nd Vehicular Technology Conference (VTC2015-Fall)*, Boston, MA, 2015, pp. 1-2.

[61] "ANSYS HFSS-High frequency electromagnetic field simulation", Oct.2016, [online] Available: http://www.ansys.com/Products/Electronics/ANSYS-HFSS.

[62] B. D. Ratner, A. S. Hoffman, F. J. Schoen, and J. E. Lemons, *Biomaterials Science: An Introduction to Materials in Medicine.* Academic Press, Aug. 2004.

[63] J. G. Proakis and M. Salehi, Digital Communications (5^{th} Ed.), McGraw Hill, 2008.

[64] Andrea Goldsmith, Wireless Communications, Cambridge University Press, 2005.

[65] M. Ilyas, O. N. Ucan, O. Bayat, X. Yang and Q. H. Abbasi, "Mathematical Modeling of Ultra Wideband in Vivo Radio Channel," in *IEEE Access*, vol. 6, pp. 20848-20854, 2018.

[66] M. Ilyas, O. Bayat and Q. H. Abbasi, "Experimental analysis of ultra wideband in vivo radio channel," *2018 26th Signal Processing and Communications Applications Conference (SIU)*, Izmir, Turkey, 2018, pp. 1-4.

[67] M. Ilyas, O. N. Ucan, O. Bayat, A. A. Nasir, M. A. Imran, A. Alomainy and Q. H. Abbasi, "Evaluation of Ultra-Wideband In-vivo Radio Channel and its Effects on System Performance," in *Transactions on Emerging Telecommunications Technologies*, (Accepted)